Nonlinear Dyn (2020) 100:1359–1378
https://doi.org/10.1007/s11071-020-05569-8

ORIGINAL PAPER

Adaptive neural impedance control for electrically driven robotic systems based on a neuro-adaptive observer

Jinzhu Peng · Shuai Ding · Zeqi Yang · Jianbin Xin

Received: 1 August 2019 / Accepted: 6 March 2020 / Published online: 18 March 2020

Abstract This paper proposes an adaptive neural impedance control (ANIC) strategy for electrically driven robotic systems, considering system uncertainties and external disturbances. For the considered robotic system, the joint velocities and armature currents are assumed to be unknown and unmeasured, and an adaptive observer is then designed to estimate its unknown states using a neural network. Based on the observed joint velocities and armature currents, an ANIC scheme is proposed and the performances of the joint positions and force tracking can be improved. We also prove that the control system is stable and all the signals in closed-loop system are bounded. Simulation examples on a two-link electrically driven robotic manipulator are presented to show the effectiveness of the proposed observer-based intelligent impedance control method.

Keywords Impedance control · Neural networks · State observer · Electrically driven robotic manipulator · Back-stepping technique

J. Peng · S. Ding · Z. Yang · J. Xin (✉)
School of Electrical Engineering, Zhengzhou University, Zhengzhou 450001, China
e-mail: j.xin@zzu.edu.cn

J. Peng
e-mail: jzpeng@zzu.edu.cn

1 Introduction

Robotic manipulators that are driven by the motors are usually referred to as electrically driven robotic manipulators (EDRM), and the voltages of the motors are control inputs of robotic manipulators [1,2]. It is pointed out that the relationship between the joint subsystem and the motor subsystem should not be ignored in the controller design [3]. If the motor dynamics is not considered, the control performance will be decreased. However, the robotic control system will become more complex provided that the relationship between the motor voltages and the torques is considered. For this integration, several powerful control methods have been developed to control the EDRM to achieve high performances.

As an intelligent method, neural network (NN) has been widely utilized to derive the intelligent-based controller for nonlinear systems with unknown dynamics [4–10]. In [4], an adaptive NN back-stepping controller was proposed to control a rigid link EDRM with the uncertainties of the mechanical and electrical dynamics. In [7], NN and adaptive bound part were combined with the model-based controller to achieve trajectory tracking for the redundant robot manipulator at the actuator level, and the proposed controller could guarantee that the trajectory tracking errors and subtask tracking errors were converged to zero, where the DC motors were controlled to provide the required torques for each joint. For the unknown system dynamics and

state constraints, He and Dong [11] proposed a fuzzy NN learning algorithm to identify uncertain system model without knowing the uncertainty and a sufficient amount of data observed in advance. Also, Zhang et al. [12] proposed a NN-based full-state feedback controller for robots with known closed-loop states. The above investigations designed the high-performance controller for robot manipulators based on the assumption of all the known or measured states, such as the joint positions and velocities and armature currents of motors. However, in the practical robotic manipulator systems, the joint velocities were often measured by the velocity sensors, which are expensive and usually contaminated by noise [13], further resulting in inaccurate armature currents of motors.

To reduce the cost and noise disturbances, effective observers were designed to replace the actual joint velocities measurement. Vo et al. [14] presented two second-order sliding mode observers to estimate the joint velocities and the system uncertainties, respectively, and the observer-based output feedback tracking controller was then designed. Yen et al. [15] presented a reduced-order observer for the flexible-joint EDRM to estimate the velocity signals, but the armature current had to be required for feedback. Liu et al. [16] designed the neuro-adaptive observers that could estimate all state variables of the flexible-joint robotic systems; however, the motor dynamic model was not included in robotic systems. Haouari et al. [17] combined the advantages of coefficients diagram method with the back-stepping procedure to control the EDRM in the presence of uncertainties associated with robot and motor dynamics, and an observer was designed to achieve the exponential stability with the position and velocity estimations. Regarding the position tracking control of EDRM based on the state observers, the above investigations did the great work. Yet, the forces of the end-effector have not been controlled. Since the control tasks have become increasingly complex, the traditional position-based tracking control methods cannot meet the compliance requirement of the industrial robots. Therefore, the force control for the end-effector of EDRM should be involved so that the high-accuracy positions and force tracking performances could be achieved.

As a force control method, the impedance control has better robustness and adaptability in comparison with other force control methods [18–23]. Baigzadehnoe et al. [22] proposed an adaptive fuzzy back-stepping position/force control approach to ensure that the signals of the closed-loop system were all uniformly ultimately bounded (UUB), where the fuzzy system was used to estimate the unknown system dynamic. Fateh [24] applied the voltage control strategy to provide the impedance control that was free from the dynamics of the robotic manipulator. Yang et al. [25] proposed an observer-based adaptive NN impedance controller to achieve the position and force tracking control for uncertain robotic manipulator, where a nonlinear velocity observer was designed to estimate the joint velocities. To further improve the performance of the controller, the motor dynamic model should be considered, and Chien [26] proposed a back-stepping-like procedure incorporating the model reference adaptive control strategy to construct the impedance controller. Moreover, the back-stepping technology has been widely used to design the tracking controller for the EDRM to guarantee the stability of the whole closed-loop system, as well as for the flexible-link robotic manipulators [26–32]. However, the force control and/or state observer-based control were usually not involved in the above controllers design.

Considering the above drawbacks, to achieve the high performances of position and force tracking control in the free space and the contact space, advanced and intelligent control methods need to be developed for the EDRM in the presence of the unknown joint velocities and the armature currents. To achieve the above benefits, this paper proposes an adaptive neural impedance control (ANIC) approach to control the EDRM based on a neuro-adaptive observer (NAO), where the force control and state observer-based control are considered simultaneously in the controller design. Consequently, the main contributions are presented as follows:

(1) The joint velocities of the robotic manipulator and the armature currents of the motors are all assumed to be unknown and unmeasured, and then, an NAO is presented to estimate the unknown system states.
(2) Based on the impedance relationship, an NAO-based ANIC method is proposed for controlling the EDRM, where the adaptive NN is utilized to estimate the system uncertainties so that the accuracy of the positions and force tracking is then improved, and a robust term is also derived to

compensate the approximation errors and disturbances.

(3) Considering the relationship between motor voltages and control torques, the proposed NAO-based ANIC scheme is designed by the backstepping technique, which can achieve position and force tracking performances when the EDRM contacts with environment.

According to the Lyapunov stability theory, the stability of the NAO-based ANIC system can be guaranteed. Finally, the simulation results show the feasibility of the proposed observer-based control method.

The rest of this paper is organized as follows. In Sect. 2, the structure of NN and the dynamic model of the EDRM with motor dynamics are addressed. In Sect. 3, the NAO and its stability are designed and analyzed, respectively. In Sect. 4, the NAO-based ANIC scheme and its stability analysis are also derived based on the observed states. Simulation results are presented in Sect. 5 to validate the effectiveness of the proposed intelligent-based observer and impedance control scheme, and the conclusions are given in Sect. 6.

2 Problem formulation and preliminaries

In this paper, $\Re$ denotes the real number set, $\Re^n$ denotes the n-dimensional vector space and $\Re^{n\times n}$ denotes the $n \times n$ real matrix space. The norm of vector $x \in \Re^n$ is defined as $\|x\| = \sqrt{x^{\mathrm{T}}x}$ and the norm of matrix $A \in \Re^{n\times n}$ is defined as $\|A\| = \mathrm{tr}(A^{\mathrm{T}}A)$. The minimum and the maximum eigenvalue of matrix A are denoted as $\lambda_{\min}(A)$ and $\lambda_{\max}(A)$, respectively. $I_{n\times n}$ denotes the identity matrix and $O_{m\times n}$ denotes the $m \times n$ zero matrix. The standard sign function is denoted as $\mathrm{sgn}(\cdot)$ and the diagonal function is denoted as $\mathrm{diag}(\cdot)$.

2.1 Description of neural network

In general, a neural network (NN) has the strong approximation ability, which has been proved theoretically that the NN can approximate any nonlinear continuous function over a compact set to arbitrary accuracy [5,7]. The structure of a three-layer NN can be described as,

$$\Psi(W, x) = W^{\mathrm{T}}\phi(x) \tag{1}$$

where $x = [x_1, \ldots, x_{N_n}]^{\mathrm{T}} \in \Re^{N_n}$ denotes the input vector, N_n denotes the input dimension, $W = [w_1, \ldots, w_{N_o}] \in \Re^{N_s\times N_o}$ denotes the weight matrix with $w_k \in \Re^{N_s}, k = 1, \ldots, N_o$, N_s denotes the number of neuron nodes and N_o denotes the output dimension, $\phi(x) = [\phi_1(x), \ldots, \phi_{N_s}(x)]^{\mathrm{T}} \in \Re^{N_s}$ denotes the activation function, and the Gaussian function is usually chosen as the hidden layer output function $\phi_j(x)$,

$$\phi_j(x) = \exp\left[-\frac{(x - c_j)^{\mathrm{T}}(x - c_j)}{{\delta_j}^2}\right] \tag{2}$$

where $j = 1, \ldots, N_s$, and c_j denotes the center of the jth neuron node, and δ_j denotes the width of the jth neuron.

In general, NN (1) is applied to approximate the continuous smooth function $f(x) : \Omega_x \to R$ over a compact set $\Omega_x \in \Re^{N_n}$, if N_s is large enough, the ideal bounded weights W^* exist, and we have,

$$f(x) = W^{*\mathrm{T}}\phi(x) + \varepsilon(x) \tag{3}$$

where $\varepsilon(x)$ is the reconstruction error. However, the ideal weight matrix W^* is generally unknown, the estimated weight matrix $\hat{W}$ is thus used to replace W^* to approximate the function $f(x)$, i.e.,

$$\hat{f}(x) = \hat{W}^{\mathrm{T}}\phi(x) \tag{4}$$

where $\hat{W}$ can be adjusted by the learning law. Assumed that there is a compact set Ω_W^*, which is defined as $\Omega_W^* = \{W^* \in \Re^{N_s\times N_o} : \|W^*\| \le E_W\}$, then the ideal weight matrix W^* can be obtained as,

$$W^* = \arg\min_{W^*\in\Omega_W^*}\{\sup \mid f(x) - \hat{W}^{\mathrm{T}}\phi(x) \mid\}. \tag{5}$$

Assumption 1 *The reconstruction error is bounded as,*

$$\|\varepsilon(\chi)\| \le \delta_\varepsilon \tag{6}$$

where δ_ε is a positive constant.

In this paper, to achieve the satisfied observe and control performances of the EDRM, the NNs will be utilized as the compensators to eliminate the system uncertainties both in the robotic systems and in the motor dynamics.

2.2 Robotic manipulator dynamics and properties

Considering the relationship between the motor voltages and the driven torques of a general n-degree of freedom (DOF) EDRM, the dynamical models of the manipulator and motor can be described as [3],

$$M(q)\ddot{q} + C(q,\dot{q})\dot{q} + G(q) + \tau_f(\dot{q}) + \tau_d = K_{\mathrm{T}} I_m - J^{\mathrm{T}}(q) F_e \quad (7)$$

$$L\dot{I}_m + R(I_m,\dot{q}) + u_e = u \quad (8)$$

where q, $\dot{q}$ and $\ddot{q} \in \Re^n$ represent the joint position vectors, velocity vectors and acceleration vectors of the robotic manipulator, respectively; $M(q) \in \Re^{n\times n}$ represents the positive definite and symmetric inertia matrix; $C(q,\dot{q}) \in \Re^{n\times n}$ represents the effect of centrifugal and Coriolis forces; $G(q) \in \Re^n$ represents the gravity vector; $\tau_f(\dot{q}) \in \Re^n$ is the friction effects; $\tau_d \in \Re^n$ denotes the bounded unknown disturbances including unknown payload dynamics and unstructured dynamics; $I_m \in \Re^n$ denotes the motor armature current; $K_{\mathrm{T}} \in \Re^{n\times n}$ denotes the positive definite constant diagonal matrix which characterizes the electromechanical conversion between the armature currents and joint torques; $J(q) \in \Re^{n\times n}$ represents the Jacobian matrix that is to transfer mapping from the join space to the task space; and $F_e \in \Re^n$ denotes the contact force at the end-effector. $L \in \Re^{n\times n}$ is the positive definite constant diagonal matrix denoting the electrical inductances; $R(I_m,\dot{q}) \in \Re^n$ represents the electrical resistances and the motor back-electromotive forces; $u \in \Re^n$ is the control input voltages; $u_e \in \Re^n$ represents the additive bounded voltage disturbances.

In general, due to the measuring errors, environment and payloads variations, it is difficult to obtain the precise values of $M(q)$, $C(q,\dot{q})$ and $G(q)$ in dynamical model (7), which include the physical parameters of manipulators such as links lengths, links masses, moments of inertial and so on. Here, we assume that the actual values $M(q)$, $C(q,\dot{q})$ and $G(q)$ satisfy the following relationships:

$$\begin{cases} M(q) = M_0(q) + \triangle M(q) \\ C(q,\dot{q}) = C_0(q,\dot{q}) + \triangle C(q,\dot{q}) \\ G(q) = G_0(q) + \triangle G(q) \end{cases} \quad (9)$$

where $M_0(q)$, $C_0(q,\dot{q})$ and $G_0(q)$ are the nominal parts and $\triangle M(q)$, $\triangle C(q,\dot{q})$ and $\triangle G(q)$ are the uncertain parts.

Then, the robotic dynamic model (7) can be represented as,

$$M_0(q)\ddot{q} + C_0(q,\dot{q})\dot{q} + G_0(q) + Y(q,\dot{q},I_m) + \tau_{\mathrm{d}} = K_{\mathrm{T}} I_m - J^{\mathrm{T}}(q) F_e \quad (10)$$

where $Y(q,\dot{q},I_m)$ can be expressed as follows,

$$\begin{aligned} Y(q,\dot{q},I_m) &= \triangle M(q)\ddot{q} + \triangle C(q,\dot{q})\dot{q} + \triangle G(q) + \tau_f(\dot{q}) \\ &= \triangle M(q)\Big[M^{-1}(q)\left(K_{\mathrm{T}} I_m - C(q,\dot{q})\dot{q} - G(q) - \tau_f(\dot{q}) - \tau_{\mathrm{d}}\right)\Big] \\ &\quad + \triangle C(q,\dot{q})\dot{q} + \triangle G(q) + \tau_f(\dot{q}) \end{aligned} \quad (11)$$

The following properties and assumptions are required for the subsequent development.

Property 1 *The inertia $M_0(q)$ is a positive definite and symmetric matrix, which is uniformly bounded and satisfied:*

$$0 \le \kappa_m I_{n\times n} \le M_0(q) \le \kappa_M I_{n\times n},\ \forall q \in \Re^n$$

where κ_m and κ_M are some positive constants.

Property 2 *The matrix $\dot{M}_0(q) - 2C_0(q,\dot{q})$ is skew symmetric, i.e.,*

$$\zeta^{\mathrm{T}}\left(\dot{M}_0(q) - 2C_0(q,\dot{q})\right)\zeta = 0,\ \forall \zeta \in \Re^n$$

Property 3 *The norm $C_0(q,\dot{q})$ is linear with respect to $\dot{q}$ such that*

$$\begin{aligned} C_0(q,\zeta+\varsigma) &= C_0(q,\zeta) + C_0(q,\varsigma) \\ C_0(q,\zeta)\varsigma &= C_0(q,\varsigma)\zeta \\ \|C_0(q,\zeta)\| &\le C_b\|\zeta\|,\ \text{for } q,\zeta,\varsigma \in \Re^n \end{aligned}$$

where C_b is a positive constant.

Assumption 2 *The unknown disturbance term τ_d of robotic model is bounded by $\|\tau_d\| \le \tau_D$, where τ_D is a positive constant.*

Assumption 3 *The unknown disturbance term u_e of motor model is bounded by $\|u_e\| \le u_E$, where u_E is a positive constant.*

Let $X \in \Re^m$ be the position vector of the end-effector of EDRM in the task space. The relation between the task space and the joint-space can be described by the following forward kinematics,

$$X = P(q) \quad (12)$$

where $P(\cdot)$ is the forward kinematic map, which is generally a nonlinear transformation between the task space and the joint-space. The velocities $\dot{X}$ of the end-effector in the task space is related to the joint velocities $\dot{q}$ as,

$$\dot{X} = J(q)\dot{q} \quad (13)$$

The corresponding Cartesian space representation of robotic dynamic model Eq. (10) can be then expressed as,

$$M^*\ddot{X} + C^*\dot{X} + G^* + F_f + F_{\tau_d} = J^{-T}K_T I_m - F_e \tag{14}$$

where X, $\dot{X}$ and $\ddot{X}$ are the position, velocity and acceleration vectors of the end-effector in Cartesian space, respectively. $\ddot{X} = J\ddot{q} + \dot{J}\dot{q}$, $M^* = J^{-T}M_0(q)J^{-1}$, $C^* = J^{-T}\left(C_0(q,\dot{q}) - M_0(q)J^{-1}\dot{J}\right)J^{-1}$, $G^* = J^{-T}G_0(q)$, $F_f = J^{-T}Y(q,\dot{q},I_m)$, $F_{\tau_d} = J^{-T}\tau_d$, and J is the Jacobian matrix that is assumed to be square and invertible. It should be noted that the generalized inverse matrix of $J(q)$ can be utilized provided that the Jacobian matrix $J(q)$ is not a square matrix [23].

Lemma 1 *According to Property 2, the matrix $\dot{M}^* - 2C^*$ is also skew-symmetric, i.e.,*

$$\zeta^T(\dot{M}^* - 2C^*)\zeta = 0,\ \forall\zeta \in \Re^m$$

The proof of this lemma can be found in "Appendix A".

Assumption 4 *The disturbance F_{τ_d} is bounded by $\|F_{\tau_d}\| \le F_D$, where F_D is a positive constant.*

Generally, the inaccuracy of the system states information and the uncertainties of the robotic and motor dynamics could decrease the control performances of the robotic system directly. In this paper, the objective is to design an observer to estimate the system states, and to design an adaptive neural impedance control method to achieve a certain position and force tracking performance based on the observed states even though there exists system uncertainties and external disturbances in EDRM.

3 Neuro-adaptive observer design and stability analysis

For the robotic system (8) and (10), assumed that q, F_e and u can be measured directly, while the velocities $\dot{q}$ and the currents I_m are unknown. In this section, a neuro-adaptive observer (NAO) is designed to estimate the unknown states of EDRM.

3.1 Neuro-adaptive observer design

Let the states be $x_1 = q$, $x_2 = \dot{q}$ and $x_3 = I_m$, the state-space model of EDRM described by Eqs. (8) and (10) can be then represented as,

$$\begin{cases} \dot{x}_1 = x_2 \\ \dot{x}_2 = M_0^{-1}(x_1)\left[-C_0(x_1,x_2)x_2 - G_0(x_1) \right. \\ \qquad \left. -Y(x_1,x_2,x_3) - \tau_d + K_T x_3 - J^T(x_1)F_e\right] \\ \dot{x}_3 = L^{-1}\left[u - R(x_2,x_3) - u_e\right] \\ y = x_1 \end{cases} \tag{15}$$

According to Property 3, it can be concluded that,

$$\begin{aligned} &C_0(x_1,x_2)x_2 - C_0(x_1,\hat{x}_2)\hat{x}_2 \\ &\quad = C_0(x_1,x_2)\hat{x}_2 + C_0(x_1,x_2)\tilde{x}_2 - C_0(x_1,\hat{x}_2)\hat{x}_2 \\ &\quad = C_0(x_1,\tilde{x}_2)(x_2 + \hat{x}_2) \end{aligned} \tag{16}$$

Then, the system state equation (15) can be rewritten as,

$$\begin{cases} \dot{x}_1 = x_2 \\ \dot{x}_2 = x_3 + f_{o1}(x_1,\hat{x}_2) + h_{o1}(x_1,x_2,x_3) + d_1 \\ \dot{x}_3 = L^{-1}u + h_{o2}(x_2,x_3) + d_2 \\ y = x_1 \end{cases} \tag{17}$$

where $f_{o1}(x_1,\hat{x}_2)$ represents the known part of the robotic model; $h_{o1}(x_1,x_2,x_3)$ and $h_{o2}(x_2,x_3)$ represent the unknown parts of the robotic model and the motor model, respectively; d_1 and d_2 represent the unknown disturbances of the robotic model and the motor model, respectively, which can be described as,

$$\begin{aligned} &f_{o1}(x_1,\hat{x}_2) \\ &\quad = M_0^{-1}(x_1)\Big[-C_0(x_1,\hat{x}_2)\hat{x}_2 - G_0(x_1) \\ &\qquad -J^T(x_1)F_e\Big] \end{aligned} \tag{18}$$

$$\begin{aligned} &h_{o1}(x_1,x_2,x_3) \\ &\quad = Y(x_1,x_2,x_3) - C_0(x_1,\tilde{x}_2)(x_2+\hat{x}_2) \\ &\qquad + \left(M_0^{-1}(x_1)K_T - I\right)x_3 \end{aligned} \tag{19}$$

$$h_{o2}(x_2,x_3) = -L^{-1}R(x_2,x_3) \tag{20}$$

$$d_1 = -M_0^{-1}(x_1)\tau_d \tag{21}$$

$$d_2 = -L^{-1}u_e \tag{22}$$

According to Assumptions 2 and 3 , it can be concluded that d_1 and d_2 are both bounded and satisfied,

$$\|d_1\| \le \frac{\tau_D}{\lambda_{\min}\left(M_0(q)\right)} \tag{23}$$

$$\|d_2\| \le \frac{u_E}{\|L\|} \tag{24}$$

The standard form of the system state equation (17) can be represented as,

$$\begin{cases} \dot{\chi}_o = \mathcal{A}\chi_o + H_o(\chi_o) + F_o(x_1, \hat{x}_2, u) + d \\ y = \mathcal{C}\chi_o \end{cases} \tag{25}$$

where $\chi_o = \left(x_1^{\mathrm{T}}, x_2^{\mathrm{T}}, x_3^{\mathrm{T}}\right)^{\mathrm{T}}$, $H_o(\chi_o) = [0, h_{o1}(\chi_o), h_{o2}(x_2, x_3)]^{\mathrm{T}}$, $F_o(x_1, \hat{x}_2, u) = \left[0, f_{o1}(x_1, \hat{x}_2), L^{-1}u\right]^{\mathrm{T}}$, $d = [0, d_1, d_2]^{\mathrm{T}}$, and

$$\mathcal{A} = \begin{bmatrix} 0 & I & 0 \\ 0 & 0 & I \\ 0 & 0 & 0 \end{bmatrix}, \quad \mathcal{C} = [I, 0, 0]$$

Considering the excellent approximation ability of NN to nonlinear function, in this scheme, the unknown function $H_o(\chi_o)$ is approximated by using NN, i.e.,

$$H_o(\chi_o) = {W_o^*}^{\mathrm{T}}\phi_o(\chi_o) + \varepsilon_o(\chi_o) \tag{26}$$

We select the Gaussian function (2) as the activation function of NN. Since the Gaussian function and the ideal weights are bounded, we have $\|\phi_o(\chi_o)\| \leq \beta_{\max}$ and $\|{W_o}^*\| \leq W_{\max}$, where the parameters $\beta_{\max}$ and $W_{\max}$ are both positive constants.

Assumed that the robotic system is stable, that is, x_1, x_2, x_3 and u are all bounded, then we denote $\hat{x}_1$, $\hat{x}_2$ and $\hat{x}_3$ as the observed values of x_1, x_2 and x_3, respectively, and we define the observed errors as $\tilde{x}_1 = x_1 - \hat{x}_1$, $\tilde{x}_2 = x_2 - \hat{x}_2$ and $\tilde{x}_3 = x_3 - \hat{x}_3$. Then, the NAO, which has the states $(\hat{x}_1^{\mathrm{T}}, \hat{x}_2^{\mathrm{T}}, \hat{x}_3^{\mathrm{T}})^{\mathrm{T}}$ and the inputs $(x_1^{\mathrm{T}}, u^{\mathrm{T}})^{\mathrm{T}}$, can be designed as follows,

$$\begin{cases} \dot{\hat{\chi}}_o = \mathcal{A}\hat{\chi}_o + \hat{W}_o^{\mathrm{T}}\phi_o(\hat{\chi}_o) + F_o(x_1, \hat{x}_2, u) + \mathcal{G}(y - \mathcal{C}\hat{\chi}_o) \\ \hat{y} = \mathcal{C}\hat{\chi}_o \end{cases} \tag{27}$$

where $\hat{\chi}_o = (\hat{x}_1^{\mathrm{T}}, \hat{x}_2^{\mathrm{T}}, \hat{x}_3^{\mathrm{T}})^{\mathrm{T}}$ is the estimate value of χ_o; $\mathcal{G}$ is the gain matrix of the observer. By choosing an appropriate matrix $\mathcal{G}$, the matrix $\mathcal{A} - \mathcal{G}\mathcal{C}$ can be a Hurwitz matrix.

Substituting Eq. (27) into Eq. (25), the system error dynamic equation of the observer can be obtained as,

$$\begin{cases} \dot{\tilde{\chi}}_o = \mathcal{A}\tilde{\chi}_o + H_o(\chi_o) - \hat{W}_o^{\mathrm{T}}\phi_o(\hat{\chi}_o) - \mathcal{G}(y - \mathcal{C}\hat{\chi}_o) + d \\ \tilde{y} = \mathcal{C}\tilde{\chi}_o \end{cases} \tag{28}$$

where $\tilde{\chi}_o = \chi_o - \hat{\chi}_o$, $\tilde{y} = y - \hat{y}$.

Since

$$\begin{aligned} & H_o(\chi_o) - \hat{W}_o^{\mathrm{T}}\phi_o(\hat{\chi}_o) \\ &= W_o^{*\mathrm{T}}\phi_o(\chi_o) + \varepsilon_o(\chi_o) - \hat{W}_o^{\mathrm{T}}\phi_o(\hat{\chi}_o) \\ &= \tilde{W}_o^{\mathrm{T}}\phi_o(\hat{\chi}_o) + W_o^{*\mathrm{T}}\left[\phi_o(\chi_o) - \phi_o(\hat{\chi}_o)\right] + \varepsilon_o(\chi_o) \\ &= \tilde{W}_o^{\mathrm{T}}\phi_o(\hat{\chi}_o) + \omega_o(\tilde{\chi}_o) + \varepsilon_o(\chi_o) \end{aligned} \tag{29}$$

where $\tilde{W}_o = W_o^* - \hat{W}_o$ is the estimated weight error, and $\omega_o(\tilde{\chi}_o)$ is the estimated error of the radial basis vector, which is defined as,

$$\omega_o(\tilde{\chi}_o) = W_o^{*\mathrm{T}}\tilde{\phi}_o(\tilde{\chi}_o) = W_o^{*\mathrm{T}}\left[\phi_o(\chi_o) - \phi_o(\hat{\chi}_o)\right] \tag{30}$$

Therefore, the system error dynamic equation of the observer can be then represented as,

$$\begin{cases} \dot{\tilde{\chi}}_o = \mathcal{A}'\tilde{\chi}_o + \tilde{W}_o^{\mathrm{T}}\phi_o(\hat{\chi}_o) + \omega_o(\tilde{\chi}_o) + \varepsilon_o(\chi_o) + d \\ \tilde{y} = \mathcal{C}\tilde{\chi}_o \end{cases} \tag{31}$$

where $\mathcal{A}' = \mathcal{A} - \mathcal{G}\mathcal{C}$ is a Hurwitz matrix, therefore, for a given positive definite matrix Q_o, there exists a positive definite matrix P_o, which is satisfied,

$$P_o\mathcal{A}' + {\mathcal{A}'}^{\mathrm{T}}P_o = -Q_o \tag{32}$$

Assumption 5 *The approximation and reconstruction errors of NN are bounded and satisfied,*

$$\|\omega_o(\tilde{\chi}_o)\| \leq E_{W_o}\delta_{\phi_o}$$

where δ_{ϕ_o} is the positive constant.

According to Eqs. (23) and (24), it can be concluded that the disturbance term d is bounded, that is, d satisfies $\|d\| \leq \delta_d$, where δ_d is a positive constant. And according to Assumptions 1 and 5, the approximation error of NN is bounded. Then, the following boundary condition will be satisfied as,

$$\|\omega_o(\tilde{\chi}_o) + \varepsilon_o(\chi_o) + d\| \leq E_{W_o}\delta_{\phi_o} + \delta_{\varepsilon_o} + \delta_d \triangleq \rho_o \tag{33}$$

where ρ_o is a positive constant.

3.2 Stability analysis

Theorem 1 *For the robotic dynamic models (10) and (8), we assume that Assumptions 1–3 and 5 are all satisfied, the NAO is designed as Eq. (27), the weights adaptive law of NN is designed as,*

$$\dot{\hat{W}}_o = k_{W_o}\left[\phi_o(\hat{\chi}_o)\tilde{y}^{\mathrm{T}}\mathcal{C} + \gamma\|\mathcal{C}\tilde{\chi}_o\|\hat{W}_o\right] \tag{34}$$

where k_{W_o} and γ are both the positive constants. Then, the designed observer is stable. Moreover, the observer error $\tilde{\chi}_o$ and adaptive weights error $\tilde{W}_o$ are both bounded.

Proof Choosing a Lyapunov function candidate as,

$$V_o = \frac{1}{2}\tilde{\chi}_o^{\mathrm{T}} P_o \tilde{\chi}_o + \frac{1}{2k_{W_o}} \mathrm{tr}\{\tilde{W}_o^{\mathrm{T}} \tilde{W}_o\} \tag{35}$$

Taking the derivative of the V_o with respect to time, then substituting Eqs. (32) and (33), yields,

$$\begin{aligned}
\dot{V}_o &= \frac{1}{2}\dot{\tilde{\chi}}_o^{\mathrm{T}} P_o \tilde{\chi}_o + \frac{1}{2}\tilde{\chi}_o^{\mathrm{T}} P_o \dot{\tilde{\chi}}_o + \frac{1}{k_{W_o}} \mathrm{tr}\{\tilde{W}_o^{\mathrm{T}} \dot{\tilde{W}}_o\} \\
&= \frac{1}{2}\tilde{\chi}_o^{\mathrm{T}} (P_o \mathcal{A}' + \mathcal{A}'^{\mathrm{T}} P_o) \tilde{\chi}_o \\
&\quad + \left[\tilde{W}_o^{\mathrm{T}} \phi_o(\hat{\chi}_o) + \omega_o(\tilde{\chi}_o) + \varepsilon_o(\chi_o) + d\right]^{\mathrm{T}} P_o \tilde{\chi}_o \\
&\quad + \frac{1}{k_{W_o}} \mathrm{tr}\{\tilde{W}_o^{\mathrm{T}} \dot{\tilde{W}}_o\} \\
&= -\frac{1}{2}\tilde{\chi}_o^{\mathrm{T}} Q_o \tilde{\chi}_o + \tilde{\chi}_o^{\mathrm{T}} P_o \tilde{W}_o^{\mathrm{T}} \phi_o(\hat{\chi}_o) \\
&\quad + \left[\omega_o(\tilde{\chi}_o) + \varepsilon_o(\chi_o) + d\right]^{\mathrm{T}} P_o \tilde{\chi}_o \\
&\quad + \mathrm{tr}\left\{\tilde{W}_o^{\mathrm{T}} \phi_o(\hat{\chi}_o) \tilde{\chi}_o^{\mathrm{T}} \mathcal{C}^{\mathrm{T}} \mathcal{C} + \tilde{W}_o^{\mathrm{T}} \gamma \|\mathcal{C}\tilde{\chi}_o\| (W_o^* - \tilde{W}_o)\right\} \\
&\leq -\frac{1}{2}\lambda_{\min}(Q_o)\|\tilde{\chi}_o\|^2 + \beta_{\max}\|P_o\|\|\tilde{W}_o\|\|\tilde{\chi}_o\| \\
&\quad + \beta_{\max}\|\mathcal{C}\|^2\|\tilde{W}_o\|\|\tilde{\chi}_o\| \\
&\quad + \gamma W_{\max}\|\mathcal{C}\|\|\tilde{W}_o\|\|\tilde{\chi}_o\| \\
&\quad - \gamma\|\mathcal{C}\|\|\tilde{W}_o\|^2\|\tilde{\chi}_o\| + \rho_o\|P_o\|\|\tilde{\chi}_o\| \\
&= -\frac{1}{2}\lambda_{\min}(Q_o)\|\tilde{\chi}_o\|^2 \\
&\quad + \frac{\left(\beta_{\max}\|P_o\| + \beta_{\max}\|\mathcal{C}\|^2 + \gamma W_{\max}\|\mathcal{C}\|\right)^2}{4\gamma\|\mathcal{C}\|}\|\tilde{\chi}_o\| \\
&\quad - \gamma\|\mathcal{C}\|\left(\|\tilde{W}_o\| \right. \\
&\quad \left. - \frac{\beta_{\max}\|P_o\| + \beta_{\max}\|\mathcal{C}\|^2 + \gamma W_{\max}\|\mathcal{C}\|}{2\gamma\|\mathcal{C}\|}\right)^2 \|\tilde{\chi}_o\| \\
&\quad + \rho_o\|P_o\|\|\tilde{\chi}_o\|
\end{aligned} \tag{36}$$

Since

$$-\gamma\|\mathcal{C}\|\left(\|\tilde{W}_o\| - \frac{\beta_{\max}\|P_o\| + \beta_{\max}\|\mathcal{C}\|^2 + \gamma W_{\max}\|\mathcal{C}\|}{2\gamma\|\mathcal{C}\|}\right)^2 \|\tilde{\chi}_o\| < 0 \tag{37}$$

Then, Eq. (36) is bounded as,

$$\begin{aligned}
\dot{V}_o &< -\frac{1}{2}\lambda_{\min}(Q_o)\|\tilde{\chi}_o\|^2 \\
&\quad + \frac{\left(\beta_{\max}\|P_o\| + \beta_{\max}\|\mathcal{C}\|^2 + \gamma W_{\max}\|\mathcal{C}\|\right)^2}{4\gamma\|\mathcal{C}\|}\|\tilde{\chi}_o\| \\
&\quad + \rho_o\|P_o\|\|\tilde{\chi}_o\|
\end{aligned} \tag{38}$$

We define,

$$\ell = \frac{\left(\beta_{\max}\|P_o\| + \beta_{\max}\|\mathcal{C}\|^2 + \gamma W_{\max}\|\mathcal{C}\|\right)^2}{4\gamma\|\mathcal{C}\|} > 0 \tag{39}$$

It can be concluded,

$$\dot{V}_o < -\frac{1}{2}\lambda_{\min}(Q_o)\|\tilde{\chi}_o\|^2 + \rho_o\|P_o\|\|\tilde{\chi}_o\| + \ell\|\tilde{\chi}_o\| \tag{40}$$

As shown from the above equations, if $\|\tilde{\chi}_o\| > (2\rho_o\|P_o\| + 2\ell)/\lambda_{\min}(Q_o) \triangleq \varsigma$, where ς is a positive constant, it can be concluded that $\dot{V}_o < 0$, that is, by selecting appropriate parameter γ, ρ_o and matrix $\mathcal{A}'$ to make ς be an arbitrarily small value to guarantee $\|\tilde{\chi}_o\| > \varsigma$. According to the Lyapunov stability theory, the observer states error $\tilde{\chi}_o$ and adaptive weight matrix error $\tilde{W}$ are bounded. □

4 NAO-based ANIC design and stability analysis

In this section, a neuro-adaptive observer (NAO)-based adaptive neural impedance control (ANIC) scheme based on backstepping method for the EDRM is developed to achieve the position and force tracking. To improve the tracking performances, the adaptive NN is used to estimate the system uncertainties of the robotic system, and a robust compensator term is derived to compensate the disturbances and approximation errors of the NN.

4.1 NAO-based ANIC scheme design

Define the vectors X and $\dot{X}$ as the position vector and velocity vector in the task space, respectively, the position tracking error E and velocity tracking $\dot{E}$ of the end-effector can be then represented as,

$$E = X_r - X,\ \dot{E} = \dot{X}_r - \dot{X} \tag{41}$$

where X_r and $\dot{X}_r$ are the reference position vector and velocity vector in the task space, respectively.

We define a filter tracking error as follows,

$$r = \dot{E} + \Lambda E^* \tag{42}$$

where $\Lambda = \Lambda^{\mathrm{T}} > 0$ is a positive matrix, and $E^* = [E_x^*, E_y^*, E_z^*]^{\mathrm{T}}$ is defined as,

$$E_i{}^* = \begin{cases} e_i & \text{(free space)} \\ e_{fi} & \text{(contact space)} \end{cases}, \ i = x, y, z \tag{43}$$

where e and e_f denote the position error in the free space and the force error in the contact space, respectively.

Remark 1 The error E^* is defined by considering the difference in the control targets of the robot in the free space and the contact space. In the free space, E^* is the position error e of the end-effector. While in the contact space, E^* is the combination of the position error e and the contact force error e_f of the end-effector.

Since the relationship between motor voltages and driven torques are considered in the EDRM, the force tracking impedance controller is then designed based on backstepping method. We define the error signals $z_1 = r$ and $z_2 = x_3 - \alpha$, where α is a virtual control signal. The unknown system states x_2 and x_3 are represented by the estimated values $\hat{x}_2 = x_2 - \tilde{x}_2$ and $\hat{x}_3 = x_3 - \tilde{x}_3$, respectively, which can be obtained by the designed NAO in Sect. 3, where $\tilde{x}_2$ and $\tilde{x}_3$ are the estimated errors. The velocity vector $\dot{X}$ in the task space is represented by the estimated velocity $\hat{\dot{X}} = \dot{X} - \tilde{\dot{X}}$, where $\tilde{\dot{X}}$ is the estimated velocity errors in task space. Then, the estimated filter tracking error can be represented as,

$$\hat{r} = \hat{\dot{E}} + \Lambda E^* \tag{44}$$

where $\hat{\dot{E}} = \dot{X}_r - \hat{\dot{X}}$. Then, the corresponding tracking errors can be modified as $\hat{z}_1 = \hat{r}$ and $\hat{z}_2 = \hat{x}_3 - \alpha$, and the system dynamic equations (14) and (8) can be rewritten as,

$$\begin{aligned} M^*\dot{\hat{z}}_1 &= -C^*\hat{z}_1 - J^{-\mathrm{T}}K_{\mathrm{T}}(\hat{z}_2 + \alpha) \\ &\quad + F_{\tau_d} + F_e + H_c(\chi_1) \end{aligned} \tag{45}$$

$$L\dot{\hat{z}}_2 = u - R(x_2, x_3) - L(\dot{\alpha} + \dot{\tilde{z}}_2) - u_e \tag{46}$$

where $\chi_1 = (X^{\mathrm{T}}, \dot{X}^{\mathrm{T}}, E^{*\mathrm{T}})^{\mathrm{T}}$, and $H_c(\chi_1)$ represents the uncertainties term of the robotic system and can be defined as,

$$\begin{aligned} H_c(\chi_1) &= M^*\big(\ddot{X}_r + \ddot{\tilde{X}} + \Lambda\dot{E}^*\big) \\ &\quad + C^*\big(\dot{X}_r + \dot{\tilde{X}} + \Lambda E^*\big) + G^* + F_f \end{aligned} \tag{47}$$

In this paper, the unknown function $H_c(\chi_1)$ is estimated by using NN, i.e.,

$$H_c(\chi_1) = {W_1^*}^{\mathrm{T}}\phi_1(\chi_1) + \varepsilon_1(\chi_1) \tag{48}$$

Similar as the NN in Sect. 3, the estimated error $\omega_1(\tilde{\chi}_1)$ can be represented as,

$$\omega_1(\tilde{\chi}_1) = {W_1^*}^{\mathrm{T}}\tilde{\phi}_1(\tilde{\chi}_1) = {W_1}^{*\mathrm{T}}\left[\phi_1(\chi_1) - \phi_1(\hat{\chi}_1)\right] \tag{49}$$

where $\tilde{\chi}_1 = \chi_1 - \hat{\chi}_1$ where $\hat{\chi}_1$ is the estimated state of χ_1, and $\tilde{W}_1 = W_1^* - \hat{W}_1$ is the weight estimated error.

Step 1 Select the virtual control signal α as the ideal I_m,

$$\alpha = K_{\mathrm{T}}^{-1}J^{\mathrm{T}}\left[K_{c1}\hat{z}_1 + \hat{W}_1^{\mathrm{T}}\phi_1(\hat{\chi}_1) + F_e + u_{c1}\right] \tag{50}$$

where K_{c1} is a positive matrix, and u_{c1} is a robust term, which will be defined later.

Then, substituting Eq. (50) into Eq. (45), yields,

$$\begin{aligned} M^*\dot{\hat{z}}_1 &= -C^*\hat{z}_1 - J^{-\mathrm{T}}K_{\mathrm{T}}\hat{z}_2 + F_{\tau_d} + H_c(\chi_1) \\ &\quad - \left[K_{c1}\hat{z}_1 + \hat{W}_1^{\mathrm{T}}\phi_1(\hat{\chi}_1) + u_{c1}\right] \end{aligned} \tag{51}$$

Then, substituting Eqs. (48) and (49) into Eq. (51), we have,

$$\begin{aligned} M^*\dot{\hat{z}}_1 &= -C^*\hat{z}_1 - K_{c1}\hat{z}_1 - J^{-\mathrm{T}}K_{\mathrm{T}}\hat{z}_2 + \tilde{W}_1^{\mathrm{T}}\phi_1(\hat{\chi}_1) \\ &\quad - \left[u_{c1} - \omega_1(\tilde{\chi}_1) - \varepsilon_1(\chi_1) - F_{\tau_d}\right] \end{aligned} \tag{52}$$

Similar as Assumptions 1 and 5, we can obtain,

$$\|\omega_1(\tilde{\chi}_1)\| \le E_{W_1}\delta_{\phi_1}, \ \|\varepsilon_1(\chi_1)\| \le \delta_{\varepsilon_1} \tag{53}$$

where δ_{ϕ_1} and δ_{ε_1} are both the positive constants. Then, according to Assumption 4 the following boundary condition will be satisfied as,

$$\begin{aligned} &\|\omega_1(\tilde{\chi}_1) + \varepsilon_1(\chi_1) + F_{\tau_d}\| \le E_{W_1}\delta_{\phi_1} + \delta_{\varepsilon_1} \\ &\quad + F_D \triangleq \rho_{c1} \end{aligned} \tag{54}$$

where ρ_{c1} is a positive constant. The robust compensation term u_{c1}, which is used to compensate the disturbances and approximation errors, can be designed as,

$$u_{c1} = \begin{cases} \rho_{c1}\frac{\hat{z}_1}{\|\hat{z}_1\|}, & \text{if } \|\hat{z}_1\| \ne 0 \\ 0, & \text{if } \|\hat{z}_1\| = 0 \end{cases} \tag{55}$$

The NN adaptive law is designed as,

$$\dot{\hat{W}}_1 = k_{W_1}\left[\phi_1(\hat{\chi}_1)\hat{z}_1 - \delta_{W_1}\hat{W}_1\right] \tag{56}$$

where k_{W_1} and δ_{W_1} are both the positive constants.

Choose a Lyapunov function candidate as,

$$V_1 = \frac{1}{2}\hat{z}_1^{\mathrm{T}} K_{\mathrm{T}}^{-1} M^* \hat{z}_1 + \frac{1}{2k_{W_1}} \mathrm{tr}\{\tilde{W}_1^{\mathrm{T}} \tilde{W}_1\} \tag{57}$$

Taking the derivative of the V_1 with respect to time and substituting Eq. (57), yields,

$$\begin{aligned}
\dot{V}_1 &= \frac{1}{2}\hat{z}_1^{\mathrm{T}} K_{\mathrm{T}}^{-1} \dot{M}^* \hat{z}_1 + \hat{z}_1^{\mathrm{T}} K_{\mathrm{T}}^{-1} M^* \dot{\hat{z}}_1 + \frac{1}{k_{W_1}} \mathrm{tr}\{\tilde{W}_1^{\mathrm{T}} \dot{\tilde{W}}_1\} \\
&= \frac{1}{2}\hat{z}_1^{\mathrm{T}} K_{\mathrm{T}}^{-1} \dot{M}^* \hat{z}_1 \\
&\quad + \hat{z}_1^{\mathrm{T}} K_{\mathrm{T}}^{-1} \Big\{ -C^* \hat{z}_1 - K_{c1} \hat{z}_1 - J^{-\mathrm{T}} K_{\mathrm{T}} \hat{z}_2 \\
&\quad + \tilde{W}_1^{\mathrm{T}} \phi_1(\hat{\chi}_1) - \big[u_{c1} - \omega_1(\tilde{\chi}_1) - \varepsilon_1(\chi_1) - F_{\tau_d} \big] \Big\} \\
&\quad + \frac{1}{k_{W_1}} \mathrm{tr}\{\tilde{W}_1^{\mathrm{T}} \dot{\tilde{W}}_1\} \\
&= \hat{z}_1^{\mathrm{T}} K_{\mathrm{T}}^{-1} \Big\{ - K_{c1} \hat{z}_1 - J^{-\mathrm{T}} K_{\mathrm{T}} \hat{z}_2 + \tilde{W}_1^{\mathrm{T}} \phi_1(\hat{\chi}_1) \\
&\quad - \big[u_{c1} - \omega_1(\tilde{\chi}_1) - \varepsilon_1(\chi_1) - F_{\tau_d} \big] \Big\} \\
&\quad + \frac{1}{k_{W_1}} \mathrm{tr}\{\tilde{W}_1^{\mathrm{T}} \dot{\tilde{W}}_1\}
\end{aligned} \tag{58}$$

Substituting Eqs. (54)–(56) into Eq. (58), and considering the fact $\dot{\tilde{W}}_1 = -\dot{\hat{W}}_1$, yields,

$$\dot{V}_1 \le -\hat{z}_1^{\mathrm{T}} K_{\mathrm{T}}^{-1} K_{c1} \hat{z}_1 - \hat{z}_1^{\mathrm{T}} J^{-\mathrm{T}} \hat{z}_2 + \delta_{W_1} \mathrm{tr}\{\tilde{W}_1^{\mathrm{T}} \hat{W}_1\} \tag{59}$$

Step 2 Now, we consider the motor dynamic equation (46), choose the ideal control input as,

$$u_{ed} = R(x_2, x_3) + L(\dot{\alpha} + \dot{\tilde{z}}_2) \tag{60}$$

and take the first derivative of Eq. (50), yields,

$$\begin{aligned}
\dot{\alpha} &= \frac{\partial \alpha}{\partial J}\dot{J} + \frac{\partial \alpha}{\partial \hat{z}_1}\dot{\hat{z}}_1 + \frac{\partial \alpha}{\partial \hat{W}_1}\dot{\hat{W}}_1 + \frac{\partial \alpha}{\partial \phi_1}\dot{\phi}_1 + \frac{\partial \alpha}{\partial F_e}\dot{F}_e \\
&= K_{\mathrm{T}}^{-1} \dot{J}^{\mathrm{T}} \Big(K_{c1} \hat{z}_1 + \hat{W}_1^{\mathrm{T}} \phi_1 + F_e + u_{c1} \Big) + \varphi_\alpha
\end{aligned} \tag{61}$$

where

$$\varphi_\alpha = K_{\mathrm{T}}^{-1} J^{\mathrm{T}} \Big(K_{c1} \dot{\tilde{z}}_1 + \dot{\hat{W}}_1^{\mathrm{T}} \phi_1 + \hat{W}_1^{\mathrm{T}} \dot{\phi}_1 + \dot{F}_e \Big) \tag{62}$$

In this scheme, another NN is used to approximate the ideal control input u_{ed} as,

$$u_{ed} = W_2^{*\mathrm{T}} \phi_2(\chi_2) + \varepsilon_2(\chi_2) \tag{63}$$

where $\chi_2 = (x_1^{\mathrm{T}}, x_2^{\mathrm{T}}, X^{\mathrm{T}}, \dot{X}^{\mathrm{T}}, E^{*\mathrm{T}}, \varphi_\alpha^{\mathrm{T}})^{\mathrm{T}}$.

Remark 2 In general, $R(x_2, x_3)$ in Eq. (60) includes the motor-related parameters like the back-EMF constants. These parameters are difficult to be measured precisely [3]. Also, the term $\dot{\alpha}$ in Eq. (60) is relatively complex, and it is hard to implement controller design directly. Therefore, the neural network is also used to approximate the control input u_{ed} in this step.

Since the joint velocity $\dot{q}$ and the armature current I_m are both estimated by the NAO, we use the estimated input $\hat{\chi}_2 = (\hat{x}_1^{\mathrm{T}}, \hat{x}_2^{\mathrm{T}}, X^{\mathrm{T}}, \hat{X}^{\mathrm{T}}, E^{*\mathrm{T}}, \varphi_\alpha^{\mathrm{T}})^{\mathrm{T}}$ to replace the χ_2. Then, the control input can be designed as,

$$u = J^{-\mathrm{T}} \hat{z}_1 - K_{c2} \hat{z}_2 + \hat{W}_2^{\mathrm{T}} \phi_2(\hat{\chi}_2) + u_{c2} \tag{64}$$

where u_{c2} is the robust compensation term.

Substitute Eq. (64) into Eq. (46), yields,

$$L\dot{\hat{z}}_2 = J^{-\mathrm{T}} \hat{z}_1 - K_{c2} \hat{z}_2 + \hat{W}_2^{\mathrm{T}} \phi_2(\hat{\chi}_2) + u_{c2} - u_{ed} - u_e \tag{65}$$

Similar as Eq. (29), one can obtain,

$$u_{ed} - \hat{W}_2^{\mathrm{T}} \phi_2(\hat{\chi}_2) = \tilde{W}_2^{\mathrm{T}} \phi_2(\hat{\chi}_2) + \omega_2(\tilde{\chi}_2) + \varepsilon_2(\chi_2) \tag{66}$$

where $\tilde{W}_2 = W_2^* - \hat{W}_2$, $\tilde{\chi}_2 = \chi_2^* - \hat{\chi}_2$, $\omega_2(\tilde{\chi}_2) = W_2^{*\mathrm{T}}[\phi_2(\chi_2) - \phi_2(\hat{\chi}_2)]$. And similar as Assumptions 1 and 5, we can assume,

$$\|\omega_2(\tilde{\chi}_2)\| \le E_{W_2} \delta_{\phi_2}, \quad \|\varepsilon_2(\chi_2)\| \le \delta_{W_2} \tag{67}$$

where δ_{ϕ_2} and δ_{W_2} are both the positive constants. Substitute Eq. (66) into Eq. (65), yields,

$$\begin{aligned}
L\dot{\hat{z}}_2 &= J^{-\mathrm{T}} \hat{z}_1 - K_{c2} \hat{z}_2 + \tilde{W}_2^{\mathrm{T}} \phi_2(\hat{\chi}_2) \\
&\quad + \big[u_{c2} - \omega_2(\tilde{\chi}_2) - \varepsilon_2(\chi_2) - u_e \big]
\end{aligned} \tag{68}$$

Since the approximation error of NN is bounded, and according to Assumption 3, it can be concluded that the following boundary condition is satisfied as,

$$\|\omega_2(\tilde{\chi}_2) + \varepsilon_2(\chi_2) + u_e\| \le E_{W_2} \delta_{\phi_2} + \delta_{\phi_2} + u_E \triangleq \rho_{c2} \tag{69}$$

where ρ_{c2} is a positive constant. The robust compensation term is derived as,

$$u_{c2} = \begin{cases} -\rho_{c2} \frac{\hat{z}_2}{\|\hat{z}_2\|}, & \text{if } \|\hat{z}_2\| \ne 0 \\ 0, & \text{if } \|\hat{z}_2\| = 0 \end{cases} \tag{70}$$

and the NN adaptive law is designed as,

$$\dot{\hat{W}}_2 = k_{W_2} \Big[\phi_2(\hat{\chi}_2) \hat{z}_2 - \delta_{W_2} \hat{W}_2 \Big] \tag{71}$$

where k_{W_2} and δ_{W_2} are all the positive constants.

Choosing a Lyapunov function candidate as,

$$V_{c2} = \frac{1}{2}\hat{z}_2^{\mathrm{T}} L \hat{z}_2 + \frac{1}{2k_{W_2}} \mathrm{tr}\{\tilde{W}_2^{\mathrm{T}} \tilde{W}_2\} \tag{72}$$

Taking the derivative of the V_{c2} with respect to time and substituting Eq. (68), yields,

$$\begin{aligned}\dot{V}_{c2} &= \hat{z}_2^{\mathrm{T}} L \dot{\hat{z}}_2 + \frac{1}{k_{W_2}} \mathrm{tr}\{\tilde{W}_2^{\mathrm{T}} \dot{\tilde{W}}_2\} \\ &= \hat{z}_2^{\mathrm{T}} \Big\{ J^{\mathrm{T}^{-1}} \hat{z}_1 - K_{c2} \hat{z}_2 + \tilde{W}_2^{\mathrm{T}} \phi_2(\hat{\chi}_2) \\ &\quad + \Big[u_{c2} - \Big(\omega_2(\tilde{\chi}_2) - \varepsilon_2(\chi_2) \Big) - u_e \Big] \Big\} \\ &\quad + \frac{1}{k_{W_2}} \mathrm{tr}\{\tilde{W}_2^{\mathrm{T}} \dot{\tilde{W}}_2\}\end{aligned} \tag{73}$$

According to the modeling error equation (69) and the robust compensation term (70), we can obtain

$$\hat{z}_2^{\mathrm{T}} \Big[u_{c2} - \Big(\omega_{c2}(\tilde{\chi}_2) - \varepsilon_2(\chi_2) \Big) - u_e \Big] \leq 0 \tag{74}$$

Then, considering the NN adaptive laws (71) and the fact $\dot{\tilde{W}}_2 = -\dot{\hat{W}}_2$, we have,

$$\hat{z}_2^{\mathrm{T}} \tilde{W}_2^{\mathrm{T}} \phi_2(\hat{\chi}_2) + \frac{1}{k_{W_2}} \mathrm{tr}\{\tilde{W}_2^{\mathrm{T}} \dot{\tilde{W}}_2\} = \delta_{W_2} \mathrm{tr}\{\tilde{W}_2^{\mathrm{T}} \hat{W}_2\} \tag{75}$$

Substituting Eqs. (74) and (75) into Eq. (73), yields,

$$\dot{V}_{c2} \leq \hat{z}_2^{\mathrm{T}} J^{-\mathrm{T}} \hat{z}_1 - \hat{z}_2^{\mathrm{T}} K_{c2} \hat{z}_2 + \delta_{W_2} \mathrm{tr}\{\tilde{W}_2^{\mathrm{T}} \hat{W}_2\}. \tag{76}$$

4.2 Stability analysis

Theorem 2 *Considering the robot dynamic Eq. (14) and motor dynamic Eq. (8) of EDRM, supposed that Assumptions 1–5 are all satisfied, the NAO-based ANIC law is designed as Eqs. (64) and (50), where the robust compensation terms are designed as Eqs. (70) and (55), and the NN adaptive laws are designed as Eqs. (71) and (56). Then, the stability of the observer-based closed-loop control system can be guaranteed. Furthermore, the error signals $\hat{z}_1$, $\hat{z}_2$ and adaptive parameter errors $\tilde{W}_i$, $i = 1, 2$ are all uniformly ultimately bounded(UUB). It means that the position error e in the free space, the force error e_f in the contact space and the velocity error $\dot{\hat{E}}$ are all bounded and can be made as small as possible.*

Proof Choosing a Lyapunov function as,

$$\begin{aligned}V_c = V_{c1} + V_{c2} &= \frac{1}{2}\hat{z}_1^{\mathrm{T}} M^* \hat{z}_1 + \frac{1}{2}\hat{z}_2^{\mathrm{T}} L \hat{z}_2 \\ &\quad + \sum_{i=1}^{2} \frac{1}{2k_{W_i}} \mathrm{tr}\{\tilde{W}_i^{\mathrm{T}} \tilde{W}_i\}\end{aligned} \tag{77}$$

Taking the derivative of the V_c with respect to time and substituting Eqs. (59) and (76), yields,

$$\begin{aligned}\dot{V}_c &= -\hat{z}_1^{\mathrm{T}} K_{\mathrm{T}}^{-1} K_{c1} \hat{z}_1 - \hat{z}_1^{\mathrm{T}} J^{-\mathrm{T}} \hat{z}_2 + \hat{z}_2^{\mathrm{T}} J^{-\mathrm{T}} \hat{z}_1 \\ &\quad - \hat{z}_2^{\mathrm{T}} K_{c2} \hat{z}_2 + \sum_{i=1}^{2} \delta_{W_i} \mathrm{tr}\{\tilde{W}_i^{\mathrm{T}} \dot{\tilde{W}}_i\} \\ &= -\hat{z}_1^{\mathrm{T}} K_{\mathrm{T}}^{-1} K_{c1} \hat{z}_1 - \hat{z}_2^{\mathrm{T}} K_{c2} \hat{z}_2 + \sum_{i=1}^{2} \delta_{W_i} \mathrm{tr}\{\tilde{W}_i^{\mathrm{T}} \hat{W}_i\}\end{aligned} \tag{78}$$

Since

$$\begin{aligned}\sum_{i=1}^{2} \delta_{W_i} \mathrm{tr}\{\tilde{W}_i^{\mathrm{T}} \hat{W}_i\} &\leq -\sum_{i=1}^{2} \frac{\delta_{W_i}}{2} \mathrm{tr}\{\tilde{W}_i^{\mathrm{T}} \tilde{W}_i\} \\ &\quad + \sum_{i=1}^{2} \frac{\delta_{W_i}}{2} \mathrm{tr}\{W_i^{*\mathrm{T}} W_i^*\}\end{aligned} \tag{79}$$

Then, Eq. (78) is bounded as,

$$\begin{aligned}\dot{V}_c &\leq -\hat{z}_1^{\mathrm{T}} K_{\mathrm{T}}^{-1} K_{c1} \hat{z}_1 - \hat{z}_2^{\mathrm{T}} K_{c2} \hat{z}_2 - \sum_{i=1}^{2} \frac{\delta_{W_i}}{2} \mathrm{tr}\{\tilde{W}_i^{\mathrm{T}} \tilde{W}_i\} \\ &\quad + \sum_{i=1}^{2} \frac{\delta_{W_i}}{2} \mathrm{tr}\{W_i^{*\mathrm{T}} W_i^*\}\end{aligned} \tag{80}$$

Define

$$\pi_c = \frac{\lambda_{\min}(Q_c)}{\lambda_{\max}(P_c)} \tag{81}$$

where

$$Q_c = \begin{bmatrix} 2K_{\mathrm{T}}^{-1} K_{c1} & 0 & 0 \\ 0 & 2K_{c2} & 0 \\ 0 & 0 & \mathrm{diag}\{\delta_{W_1}, \delta_{W_2}\} \end{bmatrix},$$

$$P_c = \begin{bmatrix} M^* & 0 & 0 \\ 0 & L & 0 \\ 0 & 0 & \mathrm{diag}\{\frac{1}{k_{W_1}}, \frac{1}{k_{W_2}}\} \end{bmatrix}$$

and

$$\sum_{i=1}^{2} \frac{\delta_{W_i}}{2} \mathrm{tr}\{{W_i^*}^{\mathrm{T}} W_i^*\} \leq \epsilon_c \tag{82}$$

where ϵ_c is a positive constant. Then, according to Eq. (72), it can be concluded that $\dot{V}_c$ is bounded as,

$$\dot{V}_c \leq -\pi_c V_c + \epsilon_c \tag{83}$$

Based on Lyapunov stability theorem, the stability of the whole closed-loop system can be achieved. Moreover, solving the inequality (83) yields,

$$0 \leq V_c(t) \leq \left[V_c(t_0) - \frac{\epsilon_c}{\pi_c} \right] e^{-\pi_c t} + \frac{\epsilon_c}{\pi_c} \tag{84}$$

It means that the error signals $\hat{z}_1$,$\hat{z}_2$ and the NN weights errors $\tilde{W}_1$,$\tilde{W}_2$ are all UUB. Furthermore, for arbitrary $\hat{r}(t_0)$, we can obtain the following equation as $t > t_0$,

$$\begin{aligned} &\|\hat{r}(t)\| = \|\hat{z}_1(t)\| \\ &\leq \sqrt{\frac{V_c(t_0) - \epsilon_c/\pi_c}{\lambda_{\min}(P_c)} \|\hat{z}_1(t_0)\|^2 e^{-\pi_c t} + \frac{2\epsilon_c}{P_c \pi_c}} \end{aligned} \tag{85}$$

From Eq. (85), the first term within the square root will converge to zero, which means that the filter tracking error $\|\hat{r}(t)\| \leq \sqrt{2\epsilon_c/(P_c\pi_c)}$ as $t \to +\infty$. Therefore, it can be concluded that the filter tracking error, which consists of the position error e in the free space, the force error e_f in the contact space and the velocity error $\dot{\tilde{E}}$, can be made as small as possible by appropriate choice of the design parameters. □

Remark 3 Due to $\dot{E} = \dot{X}_r - \dot{X}$ and $\dot{\tilde{E}} = \dot{X}_r - \dot{\hat{X}}$, the actual velocity error can be obtained as,

$$\dot{E} = \dot{\tilde{E}} - \dot{\tilde{X}} \tag{86}$$

Since the observer errors $\tilde{x}_2$ and $\tilde{x}_3$ are both bounded and are proven in Sect. 3, which means that the observed velocity error $\dot{\tilde{X}}$ in the task space is also bounded, the actual velocity error $\dot{E}$ and the armature current I_m are bounded.

Remark 4 In this paper, the NAO is designed to obtain the unknown joint velocities and armature currents. Then, considering the relationship between motor voltages and control torques, the ANIC scheme is designed by the backstepping technique to control the EDRM based on the observed velocities and the armature currents. In the designed controller, the neural networks are used to approximate the unknown functions and uncertainties, and the robust terms are designed to eliminate the effect of the approximation errors of neural network and the external disturbances. In this way, the stability of the whole system is guaranteed and the signals in the closed-loop system are all bounded, which means that the position and force tracking can be achieved when the EDRM contacts with environment.

Remark 5 The observer parameters $\mathcal{G}$, γ, ρ_o and controller parameters Λ, K_{c1}, K_{c2}, ρ_{c1}, ρ_{c2} are sensitive to the convergence rate of the observed errors and controller errors. In general, the increase the above parameters will result in a faster convergence speed. However, it is not recommended to use very large design parameters, because this may lead to a stronger noise effect. Moreover, too large or too small values of the gain parameters γ, ρ_{c1}, ρ_{c2} will lead to the overshoot. Therefore, the parameters should be adjusted carefully for achieving suitable performances of the observer and controller.

5 Simulation examples

To verify the performances of the theoretical results, in this section, the proposed NAO-based ANIC scheme is utilized to control the electrically driven 2-DOF robotic system. The matrices of robotic system (7) are described as,

$$M(q) = \begin{bmatrix} (m_1+m_2){l_1}^2 + m_2{l_2}^2 + 2m_2 l_1 l_2 c_2 & m_2({l_2}^2 + l_1 l_2 c_2) \\ m_2({l_2}^2 + l_1 l_2 c_2) & m_2{l_2}^2 \end{bmatrix}$$

$$C(q,\dot{q}) = \begin{bmatrix} -2m_2 l_1 l_2 s_2 \dot{q}_2 & m_2 l_1 l_2 s_2 \dot{q}_2 \\ m_2 l_1 l_2 s_2 \dot{q}_2 & 0 \end{bmatrix}$$

$$G(q) = \begin{bmatrix} (m_1+m_2) l_1 g c_1 + m_2 l_2 g c_{12} \\ m_2 l_2 g c_{12} \end{bmatrix},$$

and the Jacobian matrix is given as,

$$J(q) = \begin{bmatrix} -l_1 s_1 - l_2 s_{12} & -l_2 s_{12} \\ l_1 c_1 + l_2 c_{12} & l_2 c_{12} \end{bmatrix}$$

where l_1 and l_2 denote the length of link 1 and link 2, respectively; m_1 and m_2 denote the mass of link 1 and link 2, respectively; s_i represents $\sin(q_i)$, c_i represents $\cos(q_i)$, s_{ij} and c_{ij} represent $\sin(q_i + q_j)$ and $\cos(q_i + q_j)$ for $i, j = 1, 2$, respectively; g is the acceleration of gravity.

The electrical inductance vector $L = \mathrm{diag}(L_1, L_2)$, and $R(I_m, \dot{q})$ in motor dynamic model (8) is given as,

$$R(I_m, \dot{q}) = R I_m + K_B \dot{q}$$

where the positive definite diagonal matrices $R \in \Re^{n\times n}$ and $K_B \in \Re^{n\times n}$ are the electrical resistance and the motor back-electromotive forces, respectively.

Table 1 The structures and parameters of neural networks

$\Psi(W_i, \chi_i)$	0	1	2
Structure	6-20-6	6-20-2	12-20-2
Center c_j	$[-5, 5]_{20}$	$[-5, 5]_{20}$	$[-5, 5]_{20}$
Width δ_j	5	5	5
Learning law k_{W_i}	0.2	0.2	0.15
Input $\hat{\chi}_i$	$(x_1^{\mathrm{T}}, \hat{x}_2^{\mathrm{T}}, \hat{x}_3^{\mathrm{T}})$	$(X^{\mathrm{T}}, \dot{\hat{X}}^{\mathrm{T}}, E^{*\mathrm{T}})$	$(x_1^{\mathrm{T}}, \hat{x}_2^{\mathrm{T}}, X^{\mathrm{T}}, \dot{\hat{X}}^{\mathrm{T}}, E^{*\mathrm{T}}, \varphi_\alpha^{\mathrm{T}})$
Initial weights $\hat{W}_i(0)$	0	0	0

Table 2 Simulation parameters of the robotic system

Parameter	Unit	Actual values	Nominal values
l_1	m	1	0.9
l_2	m	1	1.1
m_2	kg	2	1.6
m_2	kg	3	3.3
g	m/s^2	9.8	9.8
$K_{T1} = K_{T2}$	Nm/A	10	10
$R_1 = R_2$	Ω	4	*
$K_{B1} = K_{B2}$	Nm s/rad	4	*
$L_1 = L_2$	mH	2.5	*

*Unknown value

5.1 Design procedure

To summarize the theoretical analysis in Sects. 3 and 4, the step-by-step procedures of the NAO-based ANIC scheme for robotic manipulator can be outlined as follows:

Step 1 *Select the environmental stiffness matrix* $K_e = 2000I_{2\times2}$ *and the environmental position* $x_e = 1.3$m.

Step 2 *Select the observer gain matrix* $\mathcal{G} = [120I_{2\times2}, 120I_{2\times2}, 120I_{2\times2}]^{\mathrm{T}}$ *to make* $\mathcal{A} - \mathcal{GC}$ *to be a Hurwitz matrix and select the parameter* $\gamma = 0.05$.

Step 3 *Choose* $\Lambda = 10I_{2\times2}$ *in the free space and* $\Lambda = \mathrm{diag}(0.1, 10)$ *in the contact space in Eq.* (42)*, respectively. It should be noted that only x direction is constrained.*

Step 4 *Select controller gains* $K_{c1} = 500I_{2\times2}$ *in the virtual control vector* α (50) *and* $K_{c2} = 15I_{2\times2}$ *in the control input* (64)*, and the robust term parameters are set to be* $\rho_{c1} = 20$ *and* $\rho_{c2} = 20$ *in Eqs.* (55) *and* (70)*, respectively.*

Step 5 *Construct the NNs, the detailed structure and parameters of NNs in observer and controller are shown in Table* 1.

Then, the observer and controller can be obtained from Theorems 1 and 2, respectively.

5.2 Simulation results

The parameters of the robotic system are shown in Table 2, where the nominal values are used to facilitate the nominal controller and the actual values are used to introduce the uncertainties to test the robustness of the proposed observer and controller.

The initial conditions are chosen as $q_1(0) = \pi/2$rad, $q_2(0) = \pi/3$rad and $\dot{q}_1(0) = \dot{q}_2(0) = 0$rad/s. The observed initial conditions are chosen as $\dot{\hat{q}}_1(0) = \dot{\hat{q}}_2(0) = 0$ rad/s. The desired position

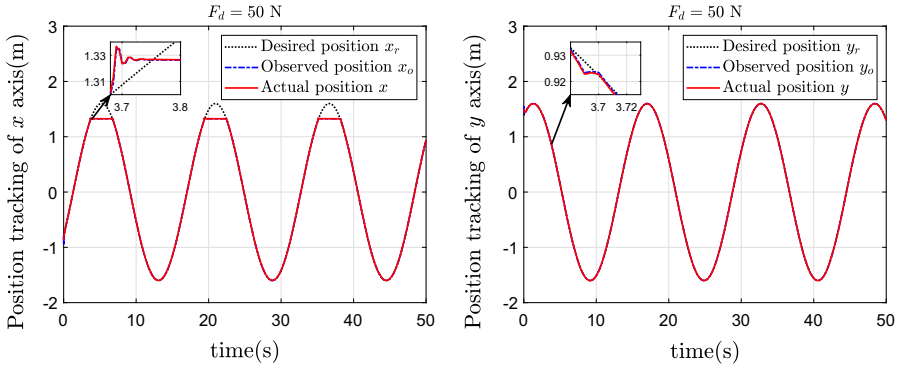

Fig. 1 Position tracking for Case 1

(a) Position tracking in the x direction **(b)** Position tracking in the y direction

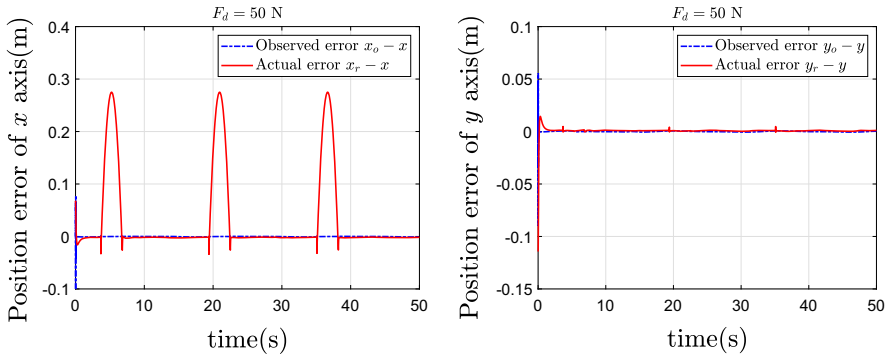

Fig. 2 Position tracking errors for Case 1

(a) Position error in the x direction **(b)** Position error in the y direction

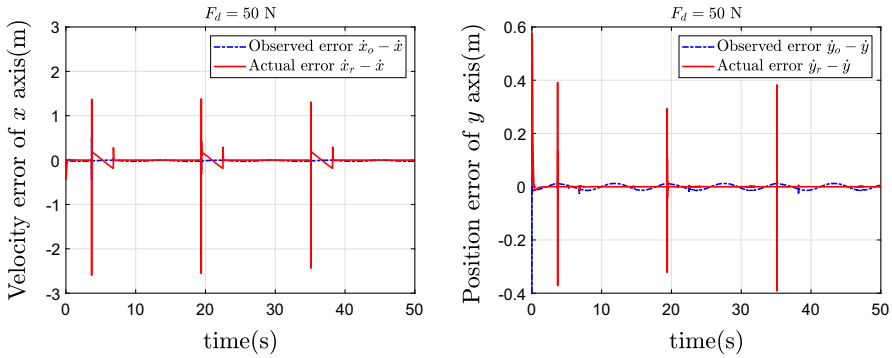

Fig. 3 Velocity tracking errors for Case 1

(a) Velocity error in the x direction **(b)** Velocity error in the y direction

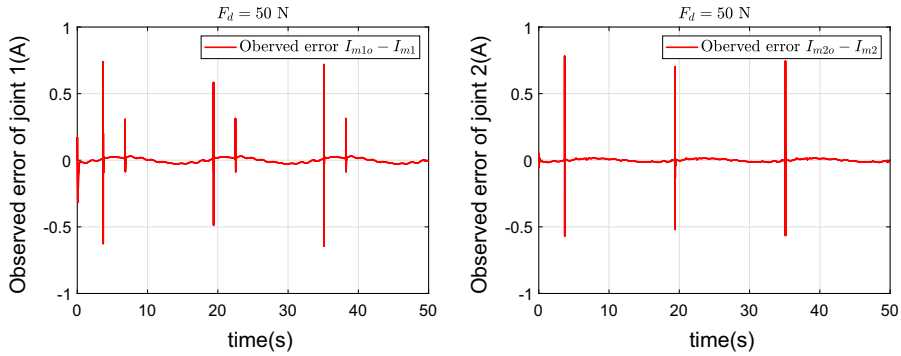

Fig. 4 Observed armature current errors for Case 1

(a) Observed armature current error of joint 1 **(b)** Observed armature current error of joint 2

and velocity of the end-effector are set as $X_r(t) = 1.6[\sin(0.4t - \pi/6), \sin(0.4t + \pi/3)]^{\mathrm{T}}$m and $\dot{X}_r(t) = 0.64[\cos(0.4t - \pi/6), \cos(0.4t + \pi/3)]^{\mathrm{T}}$m/s, respectively. To show the robustness of the proposed scheme, the friction term is $\tau_f = [3\dot{q}_1 + 0.8\mathrm{sign}(3\dot{q}_1), \dot{q}_2 + 1.1\mathrm{sign}(2\dot{q}_2)]^{\mathrm{T}}$N/m, the torque and voltage disturbances are $\tau_d = [-2\cos(2t), 2\sin(t)]^{\mathrm{T}}$ N/m and $u_e = [-0.7\cos(3t), 0.5\sin(2t)]^{\mathrm{T}}$V, respectively. In order to show the performances for tracking the constant force and the time-vary force, two simulation tests are conducted, where the constant force is set to be $F_d = [50, 0]^{\mathrm{T}}$N in Case 1 and the time-varying force is set to be $F_d = [50 + 20\sin(2t), 0]^{\mathrm{T}}$N in Case 2. To show the system robustness, additional simulation tests with complex positions and larger disturbance are also conducted in Case 3. The total simulation time is 50 s, and the sample time is 0.001 s.

Case 1 Assumed that the desired constant force is $F_d = [50, 0]^{\mathrm{T}}$N and is exerted on the end-effector

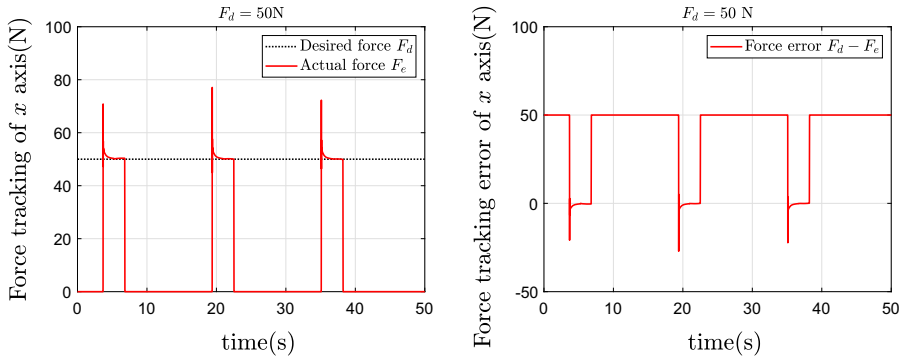

Fig. 5 Force tracking and error for Case 1

(a) Force tracking in the x direction

(b) Force error in the x direction

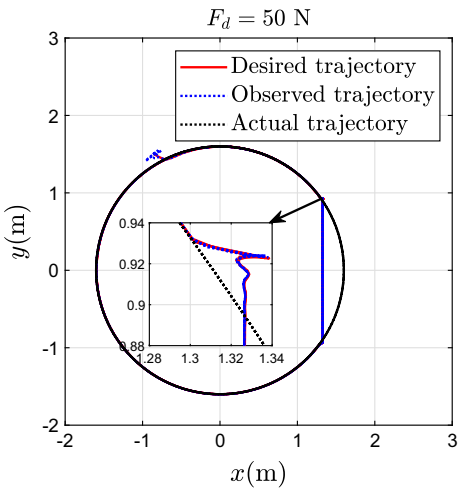

Fig. 6 Position tracking of end-effector

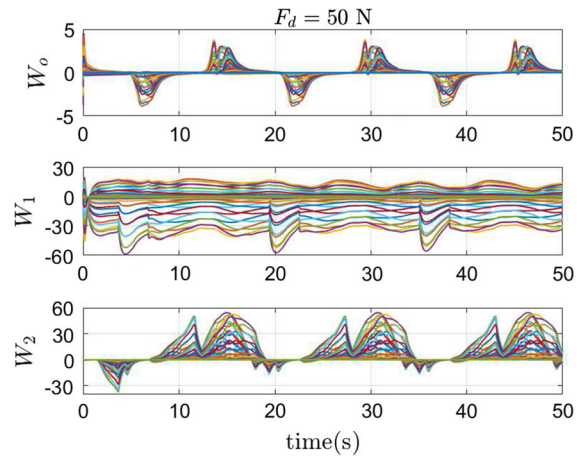

Fig. 7 Weights of neural networks

as $x \geq x_e = 1.3$ in x direction. Figure 1a, b shows the desired, observed and actual positions of the end-effector in x and y directions of the Cartesian space, respectively. Figure 2a, b shows the observed and actual position errors between the desired and actual positions in x and y directions of the Cartesian space, respectively. Figure 3a, b shows the observed and actual velocity errors in x and y directions of the Cartesian space, respectively. Figure 4a, b shows the observed current errors of joint 1 and joint 2, respectively. Figure 5a shows the force exerting on the end-effector in x direction, and Fig. 5b shows the force error in the x direction. Figure 6 shows the position tracking of the end-effector, and Fig. 7 shows the weights updating process of neural networks.

Case 2 The desired time-varying force $F_d = [50 + 20\sin(2t), 0]^{\mathrm{T}}$N is also exerted on the end-effector of EDRM to demonstrate the performance of the proposed NAO-based ANIC scheme. Similar as Case 1, Figs. 8, 9, 10, 11, 12, 13 and 14 show the simulation results, where the representations of each figure are same as Figs. 1, 2, 3, 4, 5, 6 and 7.

From the results in Case 1 and Case 2, one can see that the EDRM can work well both in the free space and in the contact space. In the free space, the tracking performances of the position (Figs. 1, 8) of the manipulator can be achieved both in x and y directions. In the contact space, the force tracking performances (Figs. 5, 12) of the manipulator can be achieved in x direction, and the position tracking performances can still be ensured in y direction. And from the position errors (Figs. 2, 9), velocity errors (Figs. 3, 10) and armature current errors (Figs. 4, 11), it is obvious that the proposed NAO-based ANIC scheme can achieve the good convergence speeds with small steady-state errors. In addition, from Figs. 7 and 14, it can be seen that all the weights of neu-

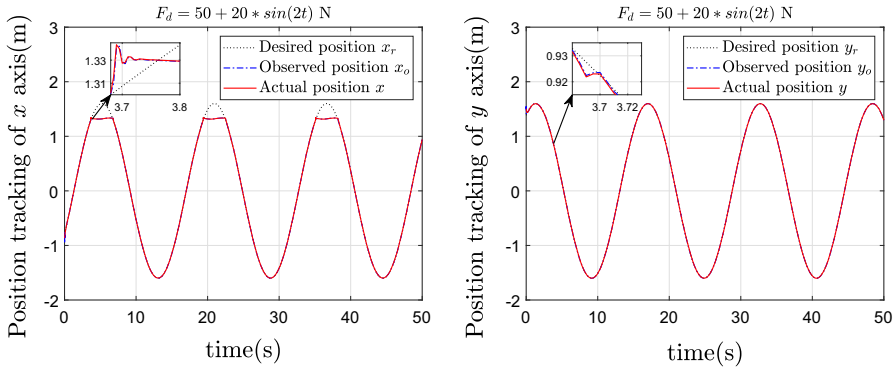

Fig. 8 Position tracking for Case 2

(a) Position tracking in the x direction **(b)** Position tracking in the y direction

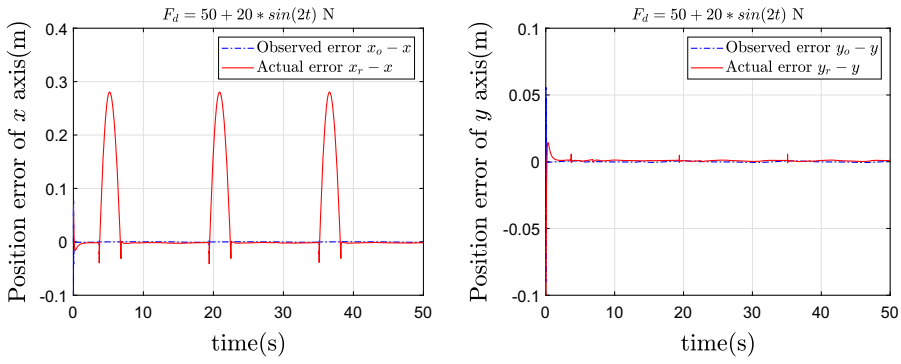

Fig. 9 Position tracking errors for Case 2

(a) Position error in the x direction **(b)** Position error in the y direction

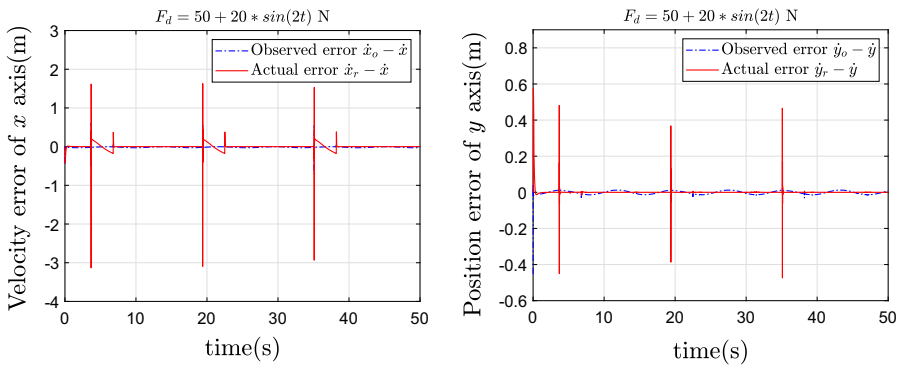

Fig. 10 Velocity tracking errors for Case 2

(a) Velocity error in the x direction **(b)** Velocity error in the y direction

ral networks in observer and controller are bounded and can converge to the optimal values quickly.

Case 3 To further verify the performances of the proposed method, more complex desired position and velocity curves are considered as $X_r(t) = [X_{r1}, X_{r2}]^{\mathrm{T}}$m and $\dot{X}_r(t) = [\dot{X}_{r1}, \dot{X}_{r2}]^{\mathrm{T}}$m/s, where X_{r1} and X_{r2} are described as Eq. (87), and $\dot{X}_{r1}$ and $\dot{X}_{r2}$ are described as Eq. (88). The initial conditions are chosen as $q_1(0) = \pi/6$rad, $q_2(0) = 2\pi/7$rad, $\dot{q}_1(0) = \dot{q}_2(0) = 0$rad/s and $\dot{\hat{q}}_1(0) = \dot{\hat{q}}_2(0) = 0$ rad/s. Also, the desired force is set to be time-varying $F_d = [50 + 20\sin(2t), 0]^{\mathrm{T}}$N that is same as Case 2. Here, compared with Case 1 and Case2, the larger torque and voltage disturbances are set as $\tau_d = [-5\cos(2t), 5\sin(t)]^{\mathrm{T}}$N/m and $u_e = [-2\cos(3t), \sin(2t)]^{\mathrm{T}}$V, respectively. Then, the larger robust gains are correspondingly chosen as $\rho_{c1} = 30$

Fig. 11 Observed armature current errors for Case 2

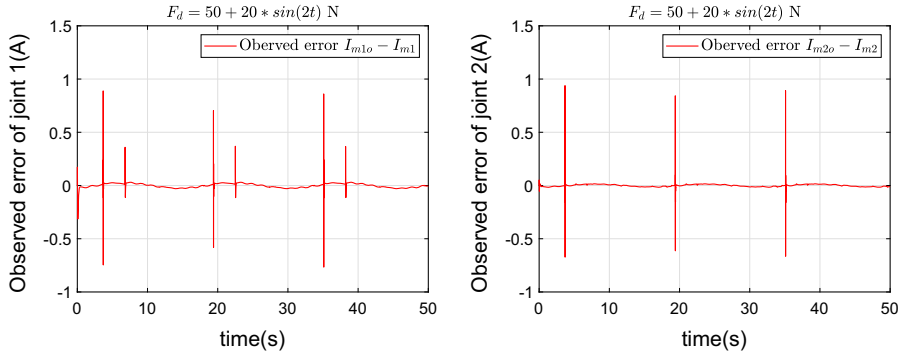

(a) Observed armature current error of joint 1

(b) Observed armature current error of joint 2

Fig. 12 Force tracking and error for Case 2

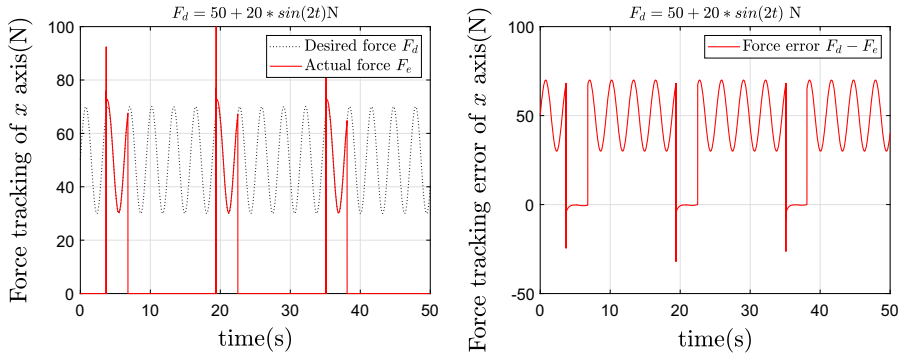

(a) Force tracking in the x direction

(b) Force error in the x direction

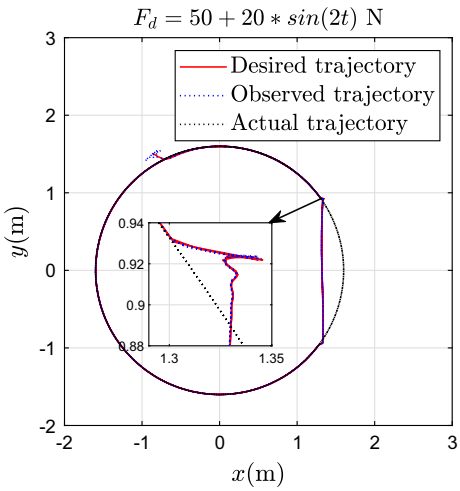

Fig. 13 Position tracking of end-effector

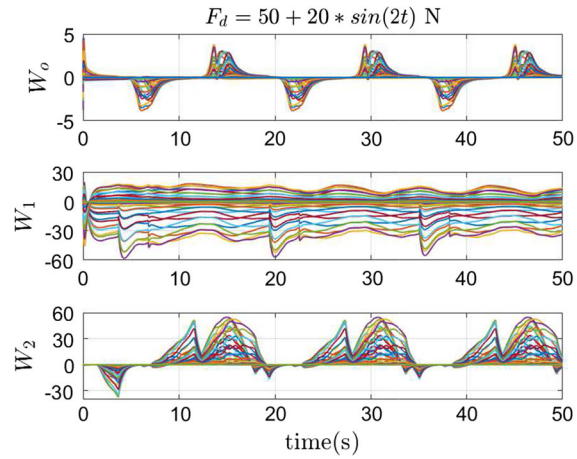

Fig. 14 Weights of neural networks

and $\rho_{c2} = 30$. Figures 15, 16, 17, 18, 19, 20 and 21 show the simulation results, where the representations of each figure are also same as Figs. 1, 2, 3, 4, 5, 6 and 7.

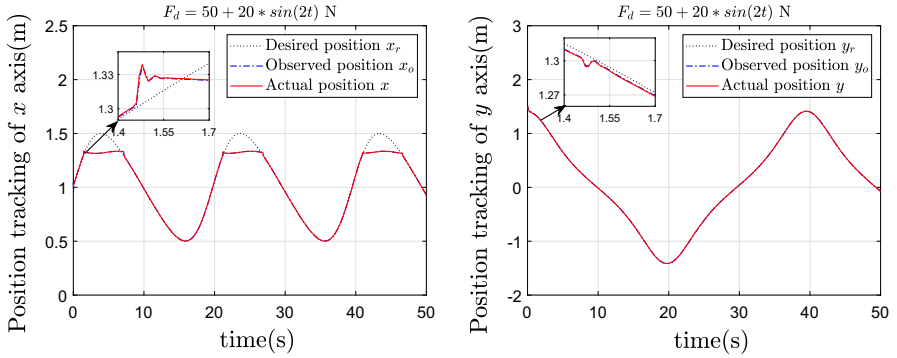

Fig. 15 Position tracking for Case 3

(a) Position tracking in the x direction **(b)** Position tracking in the y direction

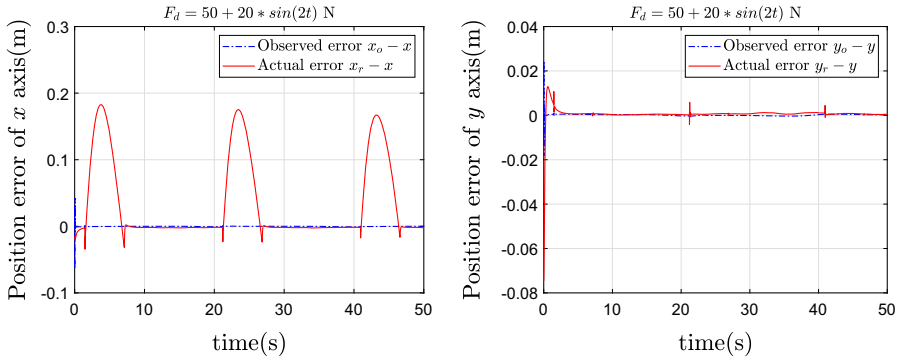

Fig. 16 Position tracking errors for Case 3

(a) Position error in the x direction **(b)** Position error in the y direction

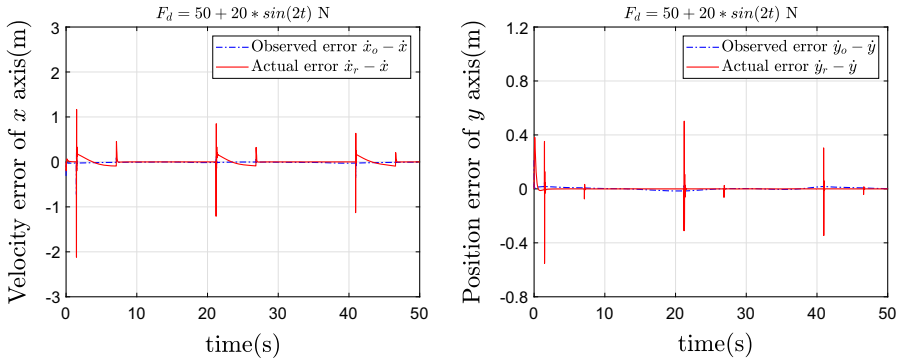

Fig. 17 Velocity tracking errors for Case 3

(a) Velocity error in the x direction **(b)** Velocity error in the y direction

$$\begin{cases} X_{r1} = \sqrt{2}\cos\left(t/(2\pi)\right)\sin\left(t/(2\pi)\right) \Big/ \sin\left(t/(2\pi)\right)\left(\left(\sin\left(t/(2\pi)\right)\right)^2 + 2\right) \\ X_{r2} = \sqrt{2}\cos\left(t/(2\pi)\right) / \left(\left(\sin\left(t/(2\pi)\right)\right)^2 + 1\right) \end{cases} \tag{87}$$

$$\begin{cases} \dot{X}_{r1} = \sqrt{2}\,\sin\left(t/2\,\pi\right)\,\left(\sin\left(t/2\,\pi\right)^2 - 3\right) \Big/ \left(2\,\pi\,\left(\sin\left(t/2\,\pi\right)^2 + 1\right)^2\right) \\ \dot{X}_{r2} = \sqrt{2}\,\left(3\,\cos\left(t/\,\pi\right) - 1\right) \Big/ \left(4\,\pi\,\left(\sin\left(t/2\,\pi\right)^2 + 1\right)^2\right) \end{cases} \tag{88}$$

Fig. 18 Observed armature current errors for Case 3

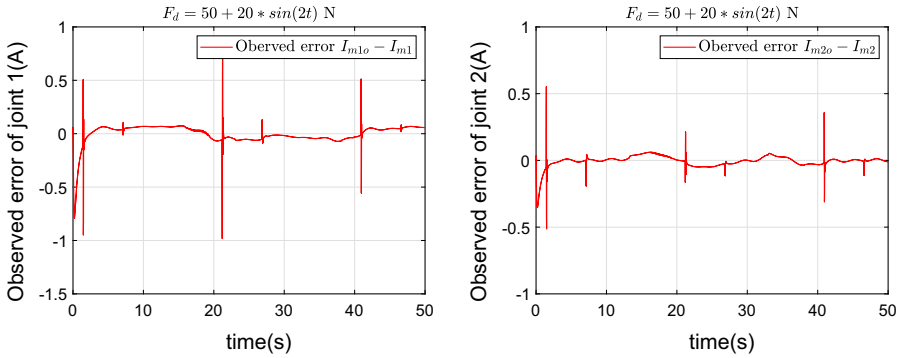

(a) Observed armature current error of joint 1

(b) Observed armature current error of joint 2

Fig. 19 Force tracking and error for Case 3

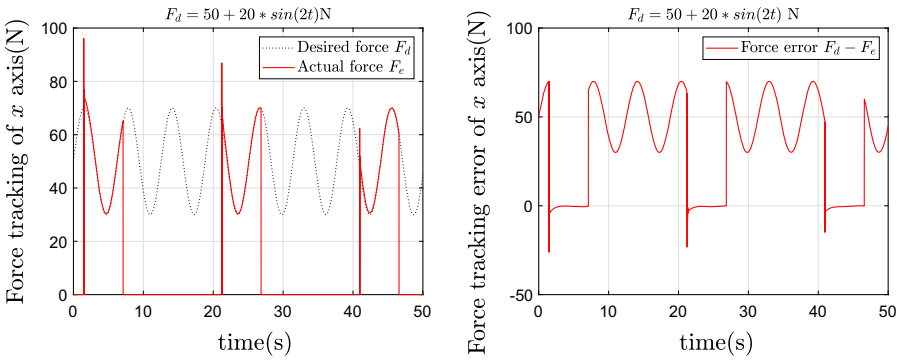

(a) Force tracking in the x direction

(b) Force error in the x direction

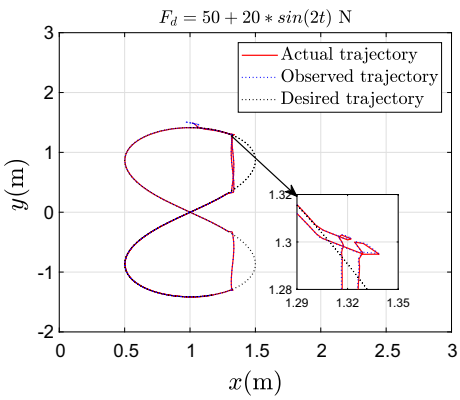

Fig. 20 Position tracking of end-effector

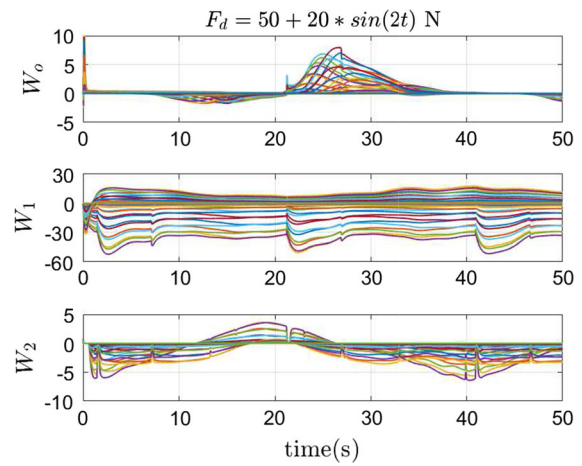

Fig. 21 Weights of neural networks

According to the simulation results of Figs. 15 and 20, we can see that the proposed NAO-based ANIC scheme can achieve the stability of the system under the complex desired positions and velocities and large disturbances. From Figs. 16, 17, 18 and 19, it can be concluded that the proposed method is still effective and the stability of the whole system can be achieved with small steady-state errors even if the large disturbances and complex desired positions are both occurred. Moreover, from Fig. 21, it can be seen that the weights of the

neural networks are bounded and can be also converged to the optimal values in finite time.

From the above results and analysis, the proposed NAO-based ANIC scheme can efficiently achieve the satisfied performances of force tracking of end-effector and the position tracking of the EDRM system without velocities and armature currents measurement.

6 Conclusions

This paper presents an adaptive neural impedance control (ANIC) method based on a neuro-adaptive observer (NAO) for the EDRM, where the joint velocities of robotic manipulator and the currents of the driven motors are assumed to be unknown and unmeasured. First, an NAO is derived to observe the unknown states of the robotic system, and the stability of NAO is also guaranteed and proven by using Lyapunov stability theory. Second, based on the observed velocities and currents, an ANIC scheme is proposed based on the back-stepping technique, where the adaptive NNs are utilized to approximate the unknown functions and uncertainties of the EDRM so that the tracking accuracy of the positions and force is improved, and the robust terms are utilized to compensate and the approximation errors of NNs and the external disturbances. Finally, the simulation tests on a two-link EDRM are conducted to demonstrate the performances of the proposed observer-based intelligent compliance control scheme.

As for future work, the proposed method will be proven experimentally and applied to the real robotic systems and other electromechanical systems. Furthermore, to enhance the intelligence of the control method, visual feedback will also be focused to facilitate the compliance control of robotic systems.

Acknowledgements This work is partially supported by the National Natural Science Foundation of China (61773351, 61703372), the Program for Science & Technology Innovation Talents in Universities of Henan Province (20HASTIT031), the Training Plan for University's Young Backbone Teachers of Henan Province (2017GGJS004), Outstanding Foreign Scientists Support Project in Henan Province of China (GZS201908) and the China Scholarship Council (201907045008).

Compliance with ethical standards

Conflict of interest The authors declare that they have no conflict of interest.

Appendix A

The proof of Lemma 1.

Taking the derivative of M^* with respect to time, we can obtain,

$$\dot{M}^* = J^{-\mathrm{T}}\dot{M}_0(q)J^{-1} - 2J^{-\mathrm{T}}M_0(q)J^{-1}\dot{J}J^{-1}. \quad (89)$$

Considering $C^* = J^{-\mathrm{T}}\left(C_0(q,\dot{q}) - M_0(q)J^{-1}\dot{J}\right)J^{-1}$ and substituting Eq. (89) and C^* into Eq. (12), yields

$$\begin{aligned}
&\zeta^{\mathrm{T}}(\dot{M}^* - 2C^*)\zeta \\
&= \zeta^{\mathrm{T}}\Big[J^{-\mathrm{T}}\dot{M}_0(q)J^{-1} \\
&\quad -2J^{-\mathrm{T}}M_0(q)J^{-1}\dot{J}J^{-1} - 2C^*\Big]\zeta \\
&= \zeta^{\mathrm{T}}\Big[J^{-\mathrm{T}}\dot{M}_0(q)J^{-1} - 2J^{-\mathrm{T}}M_0(q)J^{-1}\dot{J}J^{-1} \\
&\quad -2J^{\mathrm{T}^{-1}}\left(C_0(q,\dot{q}) - M_0(q)J^{-1}\dot{J}\right)J^{-1}\Big]\zeta \\
&= \zeta^{\mathrm{T}}\Big[J^{-\mathrm{T}}\dot{M}_0(q)J^{-1} - 2J^{-\mathrm{T}}C_0(q,\dot{q})J^{-1}\Big]\zeta \\
&= \zeta^{\mathrm{T}}\Big[J^{-\mathrm{T}}\left(\dot{M}_0(q) - 2C_0(q,\dot{q})\right)J^{-1}\Big]\zeta \\
&= 0. \qquad (90)
\end{aligned}$$

It means that the matrix $\dot{M}^* - 2C^*$ is skew symmetric.

References

1. Guldner, J., Carroll, J.J., Dawson, D.M., et al.: Robust tracking control of rigid-link electrically-driven robots. Int. J. Syst. Sci. **25**(4), 629–649 (1994)
2. Fateh, M.M., Khorashadizadeh, S.: Optimal robust voltage control of electrically driven robot manipulators. Nonlinear Dyn. **70**(2), 1445–1458 (2012)
3. Tarn, T.J., Bejczy, A.K., Yun, X., et al.: Effect of motor dynamics on nonlinear feedback robot arm control. IEEE Trans. Robot. Autom. **7**(1), 114–122 (1991)
4. Huang, S.N., Tan, K.K., Lee, T.H.: Adaptive neural network algorithm for control design of rigid-link electrically driven robots. Neurocomputing **71**(4–6), 885–894 (2008)
5. Lu, H.C., Tsai, C.H., Chang, M.H.: Radial basis function neural network with sliding mode control for robotic manipulators. In: IEEE International Conference on Systems Man and Cybernetics, pp. 1209–1215 (2010)
6. General, I.: Adaptive neural output feedback control for uncertain robot manipulators with input saturation. Complexity **2017**, 1–12 (2017)
7. Rani, M., Kumar, N.: Intelligent tracking control of redundant robot manipulators including actuator dynamics. Procedia Comput. Sci. **125**, 50–58 (2018)
8. Rahimi, H.N., Howard, I., Cui, L.: Neural adaptive tracking control for an uncertain robot manipulator with time-varying joint space constraints. Mech. Syst. Signal Process. **112**, 44–60 (2018)

9. Asl, H.J., Narikiyo, T., Kawanishi, M.: Adaptive neural network-based saturated control of robotic exoskeletons. Nonlinear Dyn. **94**(1), 123–139 (2018)
10. Peng, J., Dubay, R.: Adaptive fuzzy backstepping control for a class of uncertain nonlinear strict-feedback systems based on dynamic surface control approach. Expert Syst. Appl. **120**, 239–252 (2019)
11. He, W., Dong, Y.: Adaptive fuzzy neural network control for a constrained robot using impedance learning. IEEE Trans. Neural Netw. Learn. Syst. **29**(4), 1174–1186 (2018)
12. Zhang, S., Dong, Y., Ouyang, Y., et al.: Adaptive neural control for robotic manipulators with output constraints and uncertainties. IEEE Trans. Neural Netw. Learn. Syst. **29**(11), 5554–5564 (2018)
13. Peng, J., Liu, Y., Wang, J.: Fuzzy adaptive output feedback control for robotic systems based on fuzzy adaptive observer. Nonlinear Dyn. **78**(2), 789–801 (2014)
14. Vo, A.T., Kang, H.J., Nguyen, V.C.: An output feedback tracking control based on neural sliding mode and high order sliding mode observer. In: International Conference on Human System Interactions, pp. 161–165 (2017)
15. Yen, H.M., Li, T.H.S., Chang, Y.C.: Adaptive neural network based tracking control for electrically driven flexible-joint robots without velocity measurements. Comput. Math. Appl. **64**(5), 1022–1032 (2012)
16. Liu, X., Yang, C., Chen, Z., et al.: Neuro-adaptive observer based control of flexible joint robot. Neurocomputing **275**, 73–82 (2018)
17. Haouari, F., Bali, N., Tadjine, M., et al.: A CDM-backstepping control with nonlinear observer for electrically driven robot manipulator. Autom. Control Comput. Sci. **50**(5), 332–346 (2016)
18. Takahashi, C., Scheidt, R., Reinkensmeyer, D.: Impedance control and internal model formation when reaching in a randomly varying dynamical environment. J. Neurophysiol. **86**(2), 1047–1051 (2001)
19. Peng, J., Yang, Z., Wang, Y., et al.: Robust adaptive motion/force control scheme for crawler-type mobile manipulator with nonholonomic constraint based on sliding mode control approach. ISA Trans. **92**, 166–179 (2019)
20. Ott, C., Nakamura, Y.: Base force/torque sensing for position based Cartesian impedance control. In: IEEE/RSJ International Conference on Intelligent Robots and Systems, pp. 3244–3250 (2009)
21. Xu, Q.: Robust impedance control of a compliant microgripper for high-speed position/force regulation. IEEE Trans. Ind. Electron. **62**(2), 1201–1209 (2015)
22. Baigzadehnoe, B., Rahmani, Z., Khosravi, A., et al.: On position/force tracking control problem of cooperative robot manipulators using adaptive fuzzy backstepping approach. ISA Trans. **70**, 432–446 (2017)
23. Peng, J., Yang, Z., Ma, T.: Position/force tracking impedance control for robotic systems with uncertainties based on adaptive Jacobian and neural network. Complexity **2019**, 1–17 (2019)
24. Fateh, M.M., Babaghasabha, R.: Impedance control of robots using voltage control strategy. Nonlinear Dyn. **74**(1–2), 277–286 (2013)
25. Yang, Z., Peng, J., Liu, Y.: Adaptive neural network force tracking impedance control for uncertain robotic manipulator based on nonlinear velocity observer. Neurocomputing **331**, 263–280 (2019)
26. Chien, M.C., Huang, A.C.: Adaptive impedance controller design for flexible-joint electrically-driven robots without computation of the regressor matrix. Robotica **30**(1), 133–144 (2012)
27. Izadbakhsh, A.: Robust control design for rigid-link flexible-joint electrically driven robot subjected to constraint: theory and experimental verification. Nonlinear Dyn. **85**(2), 751–765 (2016)
28. Neria, M.R., Ortega, G.O., Castillo, N.L., et al.: On the robust trajectory tracking task for flexible-joint robotic arm with unmodeled dynamics. IEEE Access. **4**, 7816–7827 (2016)
29. Liu, H., Huang, Y., Wu, W.: Improved adaptive output feedback controller for flexible-joint robot manipulators. In: IEEE International Conference on Information and Automation, pp. 1653–1658 (2017)
30. Izadbakhsh, A.: FAT-based robust adaptive control of electrically driven robots without velocity measurements. Nonlinear Dyn. **89**(1), 289–304 (2017)
31. Lochan, K., Singh, J.P., Roy, B.K., et al.: Adaptive time-varying supertwisting global SMC for projective synchronisation of flexible manipulator. Nonlinear Dyn. **93**(4), 2071–2088 (2018)
32. Dian, S., Hu, Y., Zhao, T., et al.: Adaptive backstepping control for flexible-joint manipulator using interval type-2 fuzzy neural network approximator. Nonlinear Dyn. **97**(2), 1567–1580 (2019)